

Answers to the referee comments for article “Simultaneous assimilation of ozone profiles from multiple UV-VIS satellite instruments”

The accompanying difference document has been generated with the latexdiff program. This program visually highlights all changes in the document, so we do not repeat all edited text in these answers. At the request of referee #2, a new figure has been created instead of table 1 so other figure numbers will have changed. These new figure numbers are not highlighted by the latexdiff program. Note that references to pages, lines, figures and tables in this “Answers...” document refer to the ACP discussion paper, not to the difference paper unless otherwise noted.

1 Anonymous referee #1

1.1 Specific comments

1. In abstract, it is good to add the improvement in terms of standard deviation of the differences, which I think it is a more important criterion.

Please see the answer to specific comment 19.

2. P3, L32, Is the retrieval done at 65 km x 48 km? According to the readme document of the OMO3PRO product, it is retrieved at 13 km x 48 km although only 1 out of 5 pixels along the track is retrieved.

The readme doc the referee is probably referring to, can be found online at https://aura.gesdisc.eosdis.nasa.gov/data/Aura_OMI_Level2/OM03PR.003/doc/README.OM03PR.pdf Indeed, one in 5 scanlines in the flight direction is skipped due to limited processing resources, thus the pixel size is 13×48 km. The text of the paper has been updated.

3. P5, in section 4, what is the physical meaning of state vector x (i.e., model ozone profiles?) and measurement vector y (i.e., satellite retrievals of ozone profiles)? This is probably not clear to readers who are not familiar with data assimilation. What does the superscript f mean as it is not defined.

The state vector x is the model ozone distribution and y are the retrieved ozone profiles. Superscripts f and a are forecast and analysis respectively. The text of the paper has been updated.

4. P5, L23, H is already defined on L13, not need to repeat here.

There italic H (the observation operator) has been removed, but the boldface \mathbf{H} (the sensitivity of the observation operator with respect to the state) is still explained in the text because they refer to different quantities.

5. P5, in the last paragraph, is the linear interpolation performed actually using the cumulative profiles of ozone column instead of model profiles of partial ozone column (DU/layer)?

The linear interpolation is performed on the model partial ozone column profile. The text of the paper has been updated.

6. P6, L31, instead of using a small fraction of the retrievals, have you tried to average all retrievals to the model grid? In this way, the spatial resolution matches with the model, retrieval noise is reduced, and more retrievals are utilized to maximize the amount of retrieval information in the assimilation process.

Referee #2 (i.e. page C3) refers to this possibility as superobservations. The assimilation algorithm described in this paper requires the averaging kernel to account for the instrument sensitivity. The AK is a retrieval specific quantity and averaging AKs is not straightforward. The text of the paper has been updated.

7. P7, L26, the integration time of 1B is always 0.1875s. Do you mean that the integration time of 283-307 nm (previously part of 1A and now part of 1B) changes from 1.5s to 0.1875s? If so, please make it clear.

That is indeed what we mean and the text of the paper has been updated.

8. P8, in the paragraph of L10: the update of L0 to L1 processor corrected a bug in the noise calculation of the old L0 to L1 processing, reducing the noise by a factor of approximately $\text{SQRT}(2)$ to $\text{SQRT}(5)$ depending on the number of integrations per observation. So the noise calculation in the updated L0 to L1 processor should be correct and better. Since your estimate of noise compares quite well with the old one, do you think if the noise calculation in the updated L0 to L1 processor is wrong or is there any limitation in your approach using equation (14)? Also, the noise difference before and after the update of the L0 to L1 processor should be a factor of $\text{SQRT}(2)$ to $\text{SQRT}(5)$, not a factor of 5. Furthermore, all the OMI level 1b data have been reprocessed with the new processor. So for the OMI ozone profile product before February 1, 2010, has it been reprocessed using the new level 1b data? In Figure 2, left panel is for Feb 25, 2006 and the right panel is for Feb 5, 2010. I think that it is even better to compare the data from the same day, one with older processor and one with the updated processor.

We believe there is room for improvement in the noise calculation in the L0 to L1 processor because our approach works correctly for GOME-2 and the old OMI processor version. In figure 1 in the article, we demonstrate that an instrument feature such as the GOME-2 band 1A/1B shift is correctly detected by our approach. Therefore, we do not think there is a limitation in our approach.

According to the document ‘‘Bug fix for GDPS measurement noise calculation algorithm’’ (TN-OMIE-KNMI-935, Issue 1, 14 October 2009), the old and new error calculation are respectively:

$$\text{Noise}(i, j)_k = \sqrt{S_{\text{input}}(i, j)_k + N_{\text{co-addition}} \cdot \sigma_{\text{read-out}, k, g}^2} \quad (1)$$

$$\text{Noise}(i, j)_k = \frac{\sqrt{N_{\text{co-addition}} \cdot S_{\text{input}}(i, j)_k + N_{\text{co-addition}} \cdot \sigma_{\text{read-out}, k, g}^2}}{N_{\text{co-addition}}} \quad (2)$$

where $S_{\text{input}}(i, j)_k$ is the signal in electrons for column i , row j and channel k . $N_{\text{co-addition}}$ is the number of co-additions (i.e. 2 to 5 as the referee already mentioned) and $\sigma_{\text{read-out}, k, g}$ is the read-out noise for channel k and gain switch column identifier g . From these two equations, it follows that the noise reduction depends on the ratio of S_{input} and $\sigma_{\text{read-out}}$.

It is therefore not straightforward that the reduction should be a factor of $\sqrt{2}$ to $\sqrt{5}$ as the referee remarks.

The OMI L1b error has been updated, but the radiances have not been recalculated. No reprocessing of the ozone retrievals have been done, the new noise calculation has been used after the processor update, but not before.

We do not have data for the same day processed with the old and new processor, so unfortunately it is not possible to compare the data as the referee suggests.

9. P9, L4, what is the meaning of A in the equation?

“A” is a fit parameter used to fit the function $A \cdot t^{1/3}$ to the data in Eskes (2003) figure 2. The text of the paper has been updated.

10. Table 1 caption, it is useful to add the meaning of a (i.e., maximum relative error of the model)

Referee #2 (i.e. specific comments on page C4) prefers the table as a figure. In the caption of the new figure, we added the meaning of a .

11. P10, L22, why using fitted correlations rather than the calculated correlations? Over large distances, the calculated correlations are small and dominated by noise. Therefore the correlation was fitted and small values were set to 0.

12. In Section 5.4, what are the coincidence criteria (e.g., time difference and distance) between GOME-2/OMI and ozone sonde observations? What are the ozonesonde stations used in this study? It is good to add a table of ozonesonde locations and the number of profiles used at each location.

The coincidence criteria and table have been added to the text.

13. P11, L15-16, please make it clear what latitude bands this figure is for? Or do you mean all the data at all latitudes?

We mean the data at all latitudes. The word 'global' has been added when the figure is first mentioned in the text and to the caption itself.

14. P14, Why the 1A/1B boundary in GOME-2 change decreases the surface layer OmF and OmA as the wavelengths contributing to the surface layer retrievals are longer wavelengths (e.g., 2B) that do not change.

In a retrieval, the results for different layers are related as given by the covariance matrix and the averaging kernel. It is therefore possible that a change in the short wavelength end of the spectrum affects the results in an altitude region where the radiation itself does not penetrate. The text of the paper has been updated.

15. P15, the sudden change at the start of 2009 for GOME-2 above 10 hPa is likely due to the change of 1A/1B boundary in December 2008.

If you look very carefully at the top left panel of figure 6, change in OmF and OmA as a result of the band 1A/1B change occurs really on December 10th. The sudden changes mentioned here occur on January 1st and they are also visible in the mean OmF and OmA in figure 10 for 1-1-2011. We therefore think that the sudden changes are not related to the band 1A/1B shift. The text of the paper has been updated.

16. In section 6.1, the OmF and OmA for the assimilation of one single instrument is not mentioned and discussed in this section while the conclusion mentions that “The OmF and OmA of the simultaneous assimilation of both is between . . . (P22, L1-2).” I suggest adding OmF and/or OmA for the assimilation of one single instrument on Figures 6 and 7 and add some discussion. Also the sentence in the conclusion is not clear: the OmF and OmA values are calculated for each instrument even for simultaneous assimilation, so it is not clear about what “between” mean. Are OmF and OmA values for GOME-2/OMI of simultaneous assimilation smaller than those of single assimilation?

We did not mention the OmF and OmA for the assimilation of one single instrument because we want to focus on the simultaneous assimilation. One of the issues we encountered when preparing the article was that the OmF and OmA of GOME-2 and OMI seemed to differ, while the model validation results were comparable. However, there are different layers in the retrieval of GOME-2 and OMI, which affects the OmF and OmA. After the the profiles had been regridded to the same pressure levels (as described on p13, 17-9) the OmF and OmA differences between the two instruments largely disappeared. The line in the conclusion refers to a figure that we created before the vertical regridding and has been removed.

17. P16, L13, what do you mean “the OmF differences become so large?” Do you mean the difference between OmF for GOME-2 and OmF for OMI? Also it is not clear about “only the OMI data have changed.” Please clarify it.

The section referred to by the referee has been clarified and now reads “For the simultaneous assimilation, the assimilation results may be fluctuating between OMI and GOME-2 observations if a bias exists. This might result in higher assimilation errors. Therefore, the OmF filter (see section 4, equation 13) rejects observations from both GOME-2 and OMI, even though only the uncertainties from one of the instruments (i.e. OMI) have changed.”

18. P18, L6, in “The expected and observed OmF are somewhat closer to the 1-to-1 line” and in conclusion (P22, L2-3), Figure 11 seems to contradict to this as more data points are clearly far away from 1-to-1 line in the bottom panels. Also please add slope and correlation to show the improvement quantitatively.

Somehow, the top and bottom rows were interchanged. This has been fixed, and the parameters for the best fit line and the correlation have been added. Each panel now also has a title indicating the instrument and the model run from which the data has been used.

19. Section 6.4, because the GOME-2, OMI retrievals are bias-corrected, it is more useful to examine the standard deviations of the differences between model/assimilations and ozone sonde (or 25%/75% percentiles of the differences) than showing the median differences to demonstrate the improvement quantitatively. Please add a figure or add panels to Figure 12 to show the comparisons of these quantities for the four runs.

The deviation in the differences (whether standard deviation or 25%-75% percentile) are very similar for the four runs (free model run, gome_2+omi, gome_2 single and omi single). That is also the reason why only the error bars for the simultaneous assimilation have

been plotted in figure 12. The deviations can be derived from figure 12, and vary between 20-55 %-points between 0 and 20 km and between 10-20 %-points between 20 and 40 km.

The mean bias after correction is zero, but there is still a deviation around it (see the red error bars in figure 5). Figure 5 also shows that the deviations of the observations are smaller after the bias correction than before. Because the deviation is already indicated in Figure 12, we decided not to add extra panels. A few lines with the values of the deviation has been added to the text.

The results of the simultaneous assimilation of GOME-2 and OMI has a smaller bias but comparable spread. This is actually a very good result since the spread of the combined observations is naturally higher than that of a single instrument.

1.2 Technical comments

1. P1, L2, change “satellite” to “satellites”

Changed

2. P1, L16, change to “designated as”

Changed

3. P2, L8, change “((S)BUV)” to “SBUV”

Changed

4. P2, L13, move “observed” before “once or twice a day”

Changed

5. P2, L14, change it to “Ultraviolet”

The capitalisation of Violet was meant to show where the first V in UV-VIS came from. Ultra Violet was changed to Ultraviolet.

6. P3, L7, change “a tropospheric ozone column” to “the tropospheric ozone column”

Changed

7. P3, L16-17, change it to “and in section 3 the chemical transport model that we use for the data assimilation is described” or “and section 3 describes the chemical transport model that we use for the data assimilation”

Changed

8. P3, L32, change to “two UV”

Changed

9. P4, L30, change to “meteorological”

Changed

10. P13, L2, change “An important diagnostic . . . are the differences” to “An important diagnostic . . . is the difference”

Changed

11. P17, L5, change “OMI data is missing” to “OMI data are missing”

Changed

2 Anonymous referee #2

2.1 General comment

Page 5, line 27: “*The model grid cells are $3^\circ \times 2^\circ$, much larger than the satellite ground pixels and therefore no horizontal interpolation is needed*”. But a contribution to the representation error would make sense. And what

does the model assume for the sub-gridcell concentration distribution, just completely mixed in the cell?

We did a small experiment, where GOME-2 and OMI data were assimilated into TM5 running on a horizontal resolution of $1^\circ \times 1^\circ$ (as opposed to the standard $3^\circ \times 2^\circ$ used in the article). The total column standard deviation of the six $1^\circ \times 1^\circ$ gridcells covered by a single $3^\circ \times 2^\circ$ gridcell is much smaller than the error on the total column. Therefore, the representation error due to the large gridcells is not significant.

During the assimilation, it is assumed that the model ozone is completely mixed inside a gridcell. Therefore, the retrieved ozone profile is compared directly with the model profile of the gridcell containing the center coordinates of the retrieved ozone profile.

Page 9, lines 14-15: “These results include a representation error due to the grid cell size of the model...”. How does error growth take representation error into account? Representation depends on the observation type (GOME-2, OMI), while there seems only a single error growth.

The representation error in this quote refers to the point measurement made by sondes (i.e. “truth”) and the larger $3^\circ \times 2^\circ$ (longitude \times latitude) model grid cells. They do not refer to the observations made by GOME-2 and OMI. The sonde profile is compared to the average ozone concentration over the large model grid size, so the difference will be larger than for a smaller model grid size. Since that will lead to an overestimation of the error, we discarded sondes that were too far away from the mean. The resulting sondes were used to derive the value for a in equation 15 and table 1.

Page 15, line 3: “For these narrow-swath observations, the model is closer to the retrieved profiles”. The feels counter intuitive, unless the observation error in narrow-swath mode is much smaller.

In narrow-swath mode, the retrieved profiles have smaller pixel footprints than in normal mode. The narrow-swath width is a factor of 6 smaller than the normal swath, so the ground pixels will be 160×27 km (along track \times cross track). The pixel filtering (1 in 3 pixels for GOME-2) did not change, so more pixels will fall in the model grid cell. Therefore, the model is pulled more towards the observations and the OmF and OmA will decrease.

Page 20, line 15-16: “Both instruments have different horizontal resolutions, ...”. This issue should not be left for the discussion section only.

In section 2, it is mentioned that the size of the OMI pixels increases towards the edges of the swath. So even for a single instrument, the horizontal resolutions of the observations might be different. The different horizontal resolutions might be reflected in different uncertainties and correlations, which will affect the assimilation. We did not look specifically at this issue, which is why the second part of the sentence quoted by the referee reads “..., something that has not been taken into account in the current version of the assimilation algorithm”.

Page 20, line 18-19: “The representation error of OMI will increase towards the edges of the swath”. But if the footprint is in better agreement with the model grid size, the representation error will be smaller. See also the comment on Page 7, line 1.

The representation error will be smaller with smaller pixels, because more pixels fit in the

same area and are averaged by the assimilation algorithm.

Because it is important for the result how GOME-2 and OMI observations are weighted in the assimilation, I think the representation error deserves a more extended discussion, for example as a new section 5.2 . It is not necessary to re-run the experiments, but could the authors at least give an idea of how other representation error formulations might change the results? And what would be a proper way to improve on this; could super observations help?

The representation error actually consists of two separate components: the first regarding the satellite observations (pixel footprint) and the model gridcells, and the second regarding the model output and ozone sondes.

To get an idea of the sub-gridcell variation of the concentration, we performed a small experiment where we assimilated the same observations (i.e. GOME-2 and OMI) into TM5 running on a $1^\circ \times 1^\circ$ grid (as opposed to the standard $3^\circ \times 2^\circ$ used in the article). The total column standard deviation of the six $1^\circ \times 1^\circ$ gridcells covered by a single $3^\circ \times 2^\circ$ gridcell is much smaller than the error on the total column. Therefore, the representation error due to the large gridcells is not significant. The text of the discussion section has been updated.

Sondes are used for deriving the model error growth (see section 5.2 and equation 15). Since sondes perform point measurements and the model output is given on large gridcells, there is a representation error. This is already discussed in section 5.2, following equation 15.

Referee #1 also inquires after the possibility of using superobservations. The assimilation algorithm described in this paper requires the averaging kernel to account for the instrument sensitivity. The AK is retrieval specific quantity and averaging AKs is not straightforward. Therefore we do not think that using superobservations could help in reducing the representation error.

Finally, the case study is described very short. Why was this event chosen, is it a common test case for ozone? A bit more text would be nice, otherwise this section does not contribute much.

The atmosphere over the Tibetan plateau is highly dynamic, which makes it an interesting area to study atmospheric dynamics. Because the atmosphere is so dynamic, it is also a difficult area for modelling. This case study was chosen because it is also present in the GOME-2 observations (X. Chen, J. A. Añel, Z. Su, L. de la Torre, H. Kelder, J. van Peet, and Y. Ma. The deep atmospheric boundary layer and its significance to the stratosphere and troposphere exchange over the Tibetan Plateau. PLoS ONE, 8(2):e56909, 2 2013). The observations nicely coincide with the location of the jet stream and other dynamical features. We have updated the text of section 7 to explain better why this particular case study was selected.

2.2 Specific comments

Page 2, line 32-33: *“Second, it does not produce an estimate of the uncertainty...”*. Think this is formulated too strong. Depending on the optimization method also 4D-var could produce an estimate of the uncertainty in terms of

the inverse Hessian of the cost function. Also ensemble methods might produce an uncertainty estimate.

We meant that a 4DVAR algorithm does not directly produce an uncertainty estimate like the Kalman filter does. We agree with the referee that there are options to produce an estimate of the uncertainty, so we have changed the line in the introduction to “Second, 4DVAR does not produce a direct estimate of the uncertainty in the ozone field, although such an estimate can be derived using computationally expensive techniques.”

Page 4, line 16. What are typical DFS values for GOME-2 and OMI here? On page 6, line 5 a value of “about 5 to 6” is mentioned, is that the same for both instruments?

For the cloud free retrievals over the ozone sonde stations used in this study, the mean DFS for GOME-2 is 5.0 and for OMI 5.1. The text on page 4 has been updated.

Page 6, line 7: Is the threshold 0.1 an absolute number? Or relative to the largest singular value?

This is an absolute value. The text has been updated.

Page 7, line 1: “...the outermost pixels are neglected, because of the large are of these pixels”. Larger pixels would actually match better with the grid cell size, so that would be an argument to neglected the pixels in center of the field-of-view. So why neglecting the outermost pixels, higher retrieval errors maybe?

These pixels are neglected due to higher retrieval errors, resulting from high solar zenith angles and viewing angles.

Page 9, line 3. How is the error growth applied, as factor to the std.dev. field? What is the time t , a time step? Then better use Δt . In the formula on line 9 I see that for $t \rightarrow \infty$ then $e(t) \rightarrow a$, which from Table 1 seems to be in a range 0.22-0.34. If the error growth is a factor I would expect a value above 1.0, so that means it is an absolute value?

Equation 15 gives the absolute error at time t since the last assimilation of data for a gridcell. The equation is first used to calculate the current time t , and since in the code the model timestep is also given, the error at the end of that timestep ($t + \Delta t$) can also be calculated.

The parameter a in equation 15 is the maximum absolute error of the model at a particular altitude. In table 1, the value of a is given as a relative value of the partial column because that makes it easier to compare different altitudes. The text of the article has been updated to make this distinction clear, and the table will be replaced by a figure (see “Page 10” comment below).

Page 9, lines 15-16: “Therefore, all collocations that are more than 3σ from the mean are discarded”. This looks more like an outlier test? The reason for discarding is not clear: is it to reduce the standard deviation because it also includes a contribution from the representation error? But that is not taken into at all. Please clarify.

The error growth is determined by comparing the free model run with ozone sondes. The model runs on a $3^\circ \times 2^\circ$ (longitude \times latitude) grid, while the sondes are essentially point

sources. The difference between model and sonde will become smaller when the model resolution increases, so the current settings will overestimate the model error. In order to prevent the model error from increasing too rapidly, we decided to remove collocations that are more than 3σ from the mean. The text has been updated to clarify this issue.

Page 10: Table 1 would be more clear as figure.

The table has been converted into a figure. The table values are still present as strike-through red text because of a technical latexdiff issue.

Page 11, Figure 3: Couldn't this be used to parameterize the error growth?

In our parameterization of the error growth, the free model run (i.e. without assimilation) is compared to ozone sondes (i.e. "the truth") to derive a value for the maximum error of the model. Figure 3 is an illustration of the NMC-method for the derivation of the correlation matrix which uses only model values. Because the model error refers to the difference with the true state of the atmosphere, we believe that the output of the NMC-method should not be used for deriving the error growth.

Page 11, lines 8-10: How are the soundings extended to the top of the atmosphere?

Above the burst level of the sonde, the a priori profile was used to extend the sonde profile to the top of the atmosphere. The text has been updated.

Page 11, line 19: Number of sondes, or number of sonde observations?

It is the number of sondes, but only 10 (GOME-2) or 33 (OMI) reached the top level. The text has been updated.

Page 11, lines 11-14: The values presented here depend on the layer thickness, and do not make much sense therefore. Only relative numbers would be useful, DU/km or DU/Pa. Same holds for Figure 5.

It is true that the absolute biases in DU for GOME-2 and OMI depend on the layer thickness and can therefore not be compared directly. That is why we also give the relative biases, both in the text and in figure 5, which can be compared to each other. We therefore do not see the added value of providing biases in DU/km or DU/Pa, and only added the instrument names to the plot title as requested by the referee in the "minor corrections" section below.

Page 14, Figure 6: OmF seems always positive, is it absolute bias maybe?

It is indeed the absolute bias. There was an error in equation 16 which now has been fixed.

Page 15, line 11: "...which changes its correction parameters at the start of each year". This would be easy to solve, as mentioned later on page 21 at line 8.

An interpolation scheme to reduce the differences between the bias correction parameters for different years is something to be considered for a future version of the algorithm, as mentioned in the discussion.

Page 17, lines 3-6: Text mentions specific features for GOME-2, while Figure 10 shows results for combined assimilation. How do we see the specific fea-

tures?

The instrument specific features were visible in an earlier version of the plot which had more panels. The text has been updated.

Page 18, line 6: “...*somewhat closer to the 1-to-1 line...*”. I dont really see this back in the figure.

Plot has been updated, see answer to specific comment 18 by referee #1

Page 19, line 15: Is the representation error bigger on higher altitudes? But Figure 4 suggests longer length scales at higher altitudes.

We try to attribute the observed increase in bias observed above 10 hPa to either model or observations. But since the observations also show an increase, it is not straightforward to do so. Because the representation error contributes to the observed bias, it has been mentioned in the text. We did not try to suggest that it increases with altitude, in fact, the representation error and the length scales are unrelated. The increase in correlation observed in Figure 4 are a consequence of the stratified structure of the stratosphere.

Page 21, line 16: “...*due to lack of time and resources*”. Although probably true, this remark makes more sense in a project report than a scientific journal; please reformulate.

The last part of the sentence has been deleted.

2.3 Minor corrections

Page 3, line 22: Start new paragraph at “*GOME-2...*”

Changed

Page 8, line 21: Start new sentence at “*Instead we parameterise...*”

Changed

Page 9, lines 11-17: symbols *a* should be in Italic font.

Changed

Page 13, Figure 5: names “*GOME-2*” and “*OMI*” in the title would be useful.

Changed

Page 13, line 8: pressure does not has km as units...

The levels are defined in km, converted to hPa. Changed text.

Page 19, Figure 12: caption should mention “*validation with ozone soundings*”.

Caption now starts with “Validation of the model runs with ozone sondes...”

Simultaneous assimilation of ozone profiles from multiple UV-VIS satellite instruments

Jacob van Peet¹, Ronald van der A^{1,2}, Hennie Kelder³, and Pieternel Levelt^{1,4}

¹Royal Netherlands Meteorological Institute (KNMI), De Bilt, The Netherlands

²Nanjing University of Information Science & Technology (NUIST), Nanjing, China

³Eindhoven University of Technology, Eindhoven, The Netherlands

⁴Delft University of Technology, Delft, The Netherlands

Correspondence to: van Peet (peet@knmi.nl), van der A (avander@knmi.nl)

Abstract. A three-dimensional global ozone distribution has been derived from assimilation of ozone profiles that were observed by ~~satellites~~satellites. By simultaneous assimilation of ozone profiles retrieved from the nadir looking satellite instruments Global Ozone Monitoring Experiment 2 (GOME-2) and Ozone Monitoring Instrument (OMI), which measure the atmosphere at different times of the day, the quality of the derived atmospheric ozone field has been improved. The assimilation is using an extended Kalman filter in which chemical transport model TM5 has been used for the forecast. The combined assimilation of both GOME-2 and OMI improves upon the assimilation results of a single sensor. The new assimilation system has been demonstrated by processing 4 years of data from 2008 to 2011. Validation of the assimilation output by comparison with sondes show that biases vary between -5% and +10% between the surface and 100 hPa. The biases for the combined assimilation vary between -3% and +3% in the region between 100 and 10 hPa where GOME-2 and OMI are most sensitive. This is a strong improvement compared to direct retrievals of ozone profiles from satellite observations.

1 Introduction

Depending on the altitude, ozone in the Earth's atmosphere has different effects. In the stratosphere, ozone filters the harmful ultraviolet part from the incoming solar radiation, preventing it from reaching the surface. Near to the surface, ozone is a pollutant, which has negative effects on human health and can reduce crop yields. At the same time, ozone is a greenhouse gas with an important role in the temperature of the atmosphere.

Because of the important role ozone has in climate change, it has been designated ~~an~~as Essential Climate Variable (ECV) by the Global Climate Observing System (GCOS) of the World Meteorological Organisation (WMO) (WMO, 2010). In the GCOS report, it is stressed that the full three dimensional distribution of ozone is required.

The European Space Agency (ESA) has initiated the Climate Change Initiative (CCI) programme, which aims at long-term time series of satellite observations of the ECVs (<http://cci.esa.int/>). One of the sub-programs is the Ozone CCI project (<http://www.esa-ozone-cci.org/>) that focuses on homogenized data sets of total ozone from different sensors (Lerot et al., 2014), stratospheric ozone distribution from limb and occultation observations (e.g. Sofieva et al., 2013) and the vertical ozone distribution from nadir observations (e.g. Miles et al., 2015). Long term ozone datasets were also produced by the European

Centre for Medium-Range Weather Forecasts (ECMWF) reanalyses such as ERA-40 (Uppala et al., 2005) and its successor ERA-Interim (Dee et al., 2011). Although primarily intended for improvement of the weather forecast, the assimilation of ozone is an integral part of these reanalyses. It is described in more detail for ERA-40 in Dethof and Hólm (2004) and for ERA-Interim in Dragani (2011). Total ozone column measurements from different satellite instruments were assimilated into a chemical transport model for the Multi Sensor Reanalysis (MSR) of ozone (van der A et al., 2010, 2015), spanning a 42 year period between 1970 and 2012.

Vertical ozone measurements from space-based Ultra Violet (UV) instruments started with the Solar Backscatter UltraViolet (~~(S)-BUV~~-SBUV) instruments from 1970 onwards on different satellites (e.g. Bhartia et al., 2013). Later, satellite instruments with higher resolution and increased spectral coverage were launched, for example Global Ozone Monitoring Experiment (GOME) onboard ERS-2 in 1995 (Burrows et al., 1999), SCanning Imaging Absorption spectroMeter for Atmospheric CHartographY (SCIAMACHY) onboard Envisat in 2002 (Bovensmann et al., 1999), Ozone Monitoring Instrument (OMI) onboard Aura in 2004 (Levelt et al., 2006) and Global Ozone Monitoring Experiment 2 (GOME-2) onboard MetOpA/B in 2006/2012 (Callies et al., 2000; Munro et al., 2016). Each location on Earth is typically observed once or twice a day ~~observed~~ by these satellites, so it is not possible to get global coverage at a specific time of the day. The retrieved ozone profiles from ~~Ultra~~ ~~Violet-VISible~~-Ultraviolet-VISible (UV-VIS) nadir observations have a limited vertical resolution due to the smoothing effect in the retrieval (e.g. Rodgers, 1990). The vertical resolution varies between 7 and 15 km (see e.g. Hoogen et al., 1999). To derive gridded 3D ozone distributions at fixed time intervals we use data assimilation, which combines the information present in the model and the observations, giving the optimal estimate of the ozone concentration. Either the retrieved ozone data, or the radiance data from the instrument can be assimilated into the model. Migliorini (2012) showed that both methods are equivalent. However, assimilating retrieved ozone data considerably simplifies the observation operator and reduces the number of measurements to assimilate. Since the measurement, averaging kernel and error covariance matrix are all used in our assimilation algorithm, all information gained from the retrieval is also present in the resulting assimilated model fields.

Two commonly used types of data assimilation are 4DVAR and (ensemble) Kalman filtering. For example, ozone profiles and total columns from different instruments (such as GOME) were assimilated using a 4DVAR assimilation scheme in the production of the European Centre for Medium-Range Weather Forecasts (ECMWF) ERA-Interim reanalysis (see e.g. Dragani, 2011). The Belgian Assimilation System for Chemical Observations (BASCOE, <http://bascoe.oma.be/>, Errera et al. (2008)) is a stratospheric 4DVAR data assimilation system for multiple chemical species including ozone and nitrogen dioxide. BASCOE is used in the MACC and CAMS projects for atmospheric services, the stratospheric ozone analyses from the MACC project are evaluated in Lefever et al. (2015). Recently, BASCOE has been coupled to the Integrated Forecast System of the ECMWF (Huijnen et al., 2016). 4DVAR is well suited to assimilate large amounts of observations, and the analysis provides a smooth field at the time of the assimilation. However, there are two disadvantages of 4DVAR with respect to Kalman filter techniques. First, 4DVAR requires the development and maintenance of an adjoint model, which is a complicated process. Second, ~~it~~ 4DVAR does not produce ~~an~~-a direct estimate of the uncertainty in the ozone field, although such an estimate can be derived using computationally expensive techniques.

The model covariance matrix is an integral and essential part of a Kalman filter, but it is difficult to derive and computationally expensive in the analysis calculation. Therefore, most Kalman filter implementations try to approximate the model covariance matrix. In the ensemble Kalman filter a selection of the ensemble members can be used to approximate the model covariance (see e.g. Evensen, 2003; Houtekamer and Zhang, 2016). Miyazaki et al. (2012) used an ensemble Kalman filter to
5 assimilate different trace gas measurements from multiple satellite instruments into a chemical transport model.

In this research, we follow the Kalman filter approach described in Segers et al. (2005), where the model covariance matrix is parameterised into a time dependent standard deviation field and a time independent correlation field. The algorithm was updated and used by de Laat et al. (2009) to subtract the assimilated stratospheric ozone column from the total column in order to obtain ~~a~~the tropospheric ozone column. We have implemented several major updates and improvements in the algorithm
10 compared to the version of de Laat et al.. We check the observational error characterisation, redefine the model error growth and derive a new correlation matrix for the ozone field. The new algorithm is the first that simultaneously assimilates nadir ozone profiles from multiple high spectral resolution satellite instruments. We demonstrate the new algorithm by assimilating ozone profile observations from GOME-2 and OMI for the period 2008-2011 into the chemical transport model TM5 (e.g. Krol et al., 2005). To minimise the bias between the two instruments, we developed a bias correction based on ozone sondes to
15 be applied to the observations before assimilation. A bias correction based on total column measurements from ground stations was earlier used for the Multi Sensor Reanalysis of total ozone (van der A et al., 2015). Since we assimilate ozone profiles we require an altitude dependent bias correction for which ozone soundings are selected.

In section 2 we briefly describe the ozone profile observations, and in section 3 the chemical transport model ~~is described~~ that we use for the data assimilation is described. Section 4 gives a short overview of the assimilation algorithm, section 5
20 describes the improvements applied to the assimilation algorithm and the results will be shown in section 6. In section 7 we demonstrate the performance of the assimilation algorithm over the Tibetan Plateau. A discussion of the results is given in section 8 and the conclusions are presented in section 9.

2 Observations

Data from the UV-VIS satellite instruments GOME-2 and OMI are available for the last 10 years.~

25 GOME-2 (Callies et al., 2000; Munro et al., 2016) was launched on-board METOP-A in 2006. The instrument measures the solar light reflected by the Earth's atmosphere between 250 and 790 nm. For the retrievals used in this research, the radiance measurements are binned in the cross track and along track directions such that the ground pixels measure approximately 160×160 km. The ozone profiles for GOME-2 are retrieved with the OPERA retrieval algorithm, which is described in (van Peet et al., 2014). We increased the number of layers in this study from 16 to 32 for more accurate radiative transfer
30 model results.

OMI (Levelt et al., 2006) was launched on-board Aura in 2004. The instrument measures the solar light reflected by Earth's atmosphere between 270 and 500 nm. One important difference between OMI and GOME-2 is that OMI does not use a scanning mirror like GOME-2, but a fixed 2D CCD detector. One dimension of the detector is used to cover the spectral range, the other

is used to cover the cross-track direction. The ground pixels for the profiles retrieved from the UV-VIS spectrum measure approximately 65.13×48 km, ~~with the size in nadir.~~ Note that only 1 in 5 scanlines is retrieved. The size of the ground pixels is increasing towards the edge of the swath. OMI has two ~~UV-VIS-UV~~ channels that are used in ozone profile retrieval: UV1 and UV2. UV1 has thirty cross-track pixels, while UV2 has sixty cross-track pixels. The UV2 pixels are therefore averaged to coincide with the UV1 pixels. A description of the OMI ozone retrieval algorithm and validation results with respect to ground measurements and other satellite instruments can be found in Kroon et al. (2011).

The algorithms used to retrieve the ozone profiles from GOME-2 and OMI are both based on an optimal estimation technique. The state of the atmosphere is given by the state vector x , while the measurement is given by the measurement vector y and error ϵ . These two vectors are related by the forward model F according to $y = F(x) + \epsilon$. Following the maximum a-posteriori approach (Rodgers, 2000), the solution is given by:

$$\hat{x} = x_a + A(x_t - x_a) + G\epsilon \quad (1)$$

$$\hat{S} = (I - A)S_a \quad (2)$$

$$A = GK = S_a K^T (KS_a K^T + S_\epsilon)^{-1} K \quad (3)$$

where \hat{x} is the retrieved state vector, x_a is the a priori, A is the averaging kernel, x_t is the “true” state of the atmosphere, G is the gain matrix ($S_a K^T (KS_a K^T + S_\epsilon)^{-1}$), $G\epsilon$ the retrieval noise, \hat{S} is the retrieved covariance matrix, I is the identity matrix, S_a is the a priori covariance matrix, K is the weighting function matrix or Jacobian (it gives the sensitivity of the forward model to the state vector) and S_ϵ is the measurement covariance matrix.

The averaging kernel can also be written as $A = \partial \hat{x} / \partial x_t$ and gives the sensitivity of the retrieval to the true state of the atmosphere. The trace of A gives the degrees of freedom for the signal (DFS). For the cloud free retrievals over the ozone sonde stations used in this study, the mean DFS for GOME-2 is 5.0 and for OMI 5.1. When the DFS is high, the retrieval has learned more from the measurement than in the case of a low DFS, when most of the information in the retrieval will depend on the a priori. The total DFS can be regarded as the total number of independent pieces of information in the retrieved profile. The rows of A indicate how the true profile is smoothed out over the layers in the retrieval and are therefore also called smoothing functions. Ideally, the smoothing functions peak at the corresponding level and the half-width is a measure for the vertical resolution of the retrieval.

Because the sensitivity of the retrieval to the vertical ozone distribution is represented by the averaging kernel, it is important to include the averaging kernel in the assimilation algorithm. Together the retrieved state vector, averaging kernel and error covariance matrix represent all information gained from the retrieval (Migliorini, 2012).

3 Chemical transport model TM5

The model used in the assimilation is a global chemistry transport model called TM5 (Tracer Model, version 5), see Krol et al. (2005) for an extended description. The (tropospheric) chemistry of TM5 has been evaluated in Huijnen et al. (2010) and included into the integrated forecasting system of the ECMWF (Flemming et al., 2015).

In the current model setup used for the assimilation of the ozone profiles, TM5 runs globally with grid cells of 3° longitude \times 2° latitude, on 45 pressure levels. The pressure levels are a subset of the 91 level pressure grid from the European Centre for Medium-Range Weather Forecasts (ECMWF). The ~~meteo-~~meteorological data used to drive the TM5 tracer transport are taken from the ECMWF operational analysis fields, produced on these 91 pressure levels.

5 Above 230 hPa, ozone chemistry is parameterised according to the equations described by Cariolle and Teyssère (2007), using the parameters of version 2.1. In the troposphere, the ozone concentrations are nudged towards the Fortuin & Kelder climatology (Fortuin and Kelder, 1998), with a relaxation time that increases from 0 days at 230 hPa to 14 days at 500 hPa and lower. No other trace gasses are modelled in this setup, which makes this version of TM5 fast and computationally cheap. Ozone concentrations are prevented from following the model equilibrium state too closely by the frequent confrontation of
10 the model with the observations during the assimilation process.

4 Assimilation algorithm

The assimilation algorithm uses a Kalman filter, and is described in Segers et al. (2005). The state vector ~~x_i~~ (i.e. the ozone distribution at time $t = i$) and the measurement vector ~~y_i~~ (i.e. the retrieved profiles at time $t = i$) are given by:

$$x_{i+1} = M(x_i) + w_i, \quad w_i \sim N(0, Q_i) \quad (4)$$

$$15 \quad y_i = H(x_i) + v_i, \quad v_i \sim N(0, R_i) \quad (5)$$

where M is the model that propagates the state vector in time. It has an associated uncertainty w , which is assumed to be normally distributed with zero mean and covariance matrix Q . The observation operator H , which includes the averaging kernel, gives the relation between x and y . The uncertainty in y is given by v , which is also assumed to have zero mean and covariance matrix R (which is identical to \hat{S} in the retrieval equations). In matrix notation, the propagation of the state vector
20 and its covariance matrix (P) are given by:

$$x_{i+1}^f = M(x_i^a) \quad (6)$$

$$P_{i+1}^f = M P_i^a M^T + Q_i \quad (7)$$

where x^f and x^a is the are the forecast and analysis state vector x at time $t = i$, i.e. before and after assimilation of the observations. The observations are assimilated according to:

$$25 \quad x_i^a = x_i^f + K_i \left(y_i - H(x_i^f) \right) \quad (8)$$

$$P_i^a = (I - K_i H_i) P_i^f \quad (9)$$

$$K_i = P_i^f H_i^T \left(H_i P_i^f H_i^T + R_i \right)^{-1} \quad (10)$$

where K is called the Kalman gain matrix ~~and H the observation operator. The~~ and the matrix H is the sensitivity of the observation operator with respect to the state.

The observation operator interpolates the model field to the observation location, converts the model units to the retrieval units and takes the smoothing of the satellite instruments into account by incorporating the averaging kernel. The model grid cells are $3 \times 2^\circ$ (longitude \times latitude), much larger than the satellite ground pixels and therefore no horizontal interpolation is needed. The model profile, expressed DU/layer, is converted to the pressure levels of the retrieval grid by applying a simple linear interpolation in the $^{10}\log(\text{hPa})$ domain. For example, if the L2 profile layer overlaps with three model layers for 20, 100 and 30%, the interpolated model partial column is $0.2*DU_1+1.0*DU_2+0.3*DU_3$ (where DU_i is the partial column for layer i). Finally, the observation operator H is formed by applying the averaging kernel \mathbf{A} to the difference between the state vector x and the a-priori profile y_a used in the retrieval:

$$H(x) = \mathbf{A}(\mathbf{B}\mathbf{C}x - y_a) \quad (11)$$

with \mathbf{C} the unit conversion (from the models kg/gridcell to the observations DU/layer), \mathbf{B} the vertical interpolation. The sensitivity matrix \mathbf{H} used in equations (9) and (10) is constructed as $\mathbf{H} = \mathbf{A}\mathbf{B}\mathbf{C}$.

In general, the number of elements in an ozone profile is much larger than the degrees of freedom (about 5 to 6). We can therefore reduce the number of data points per profile by taking the singular value decomposition of the \mathbf{A} , and only retain the vectors with a singular value larger than 0.1 (this is an absolute threshold, and not relative to the maximum singular value).

The profiles and matrices are transformed accordingly.

The computational cost of the assimilation algorithm can be further reduced by minimising the size of the model covariance matrix \mathbf{P} . The TM5 model runs in the current setup on a horizontal grid of $2^\circ \times 3^\circ$ (latitude \times longitude) on 44 layers, which makes the size of the covariance matrix $(475200)^2$ elements. A number of different approaches exist to minimise the size of the model covariance matrix. For example, in Eskes et al. (2003), the number of dimensions is reduced by only assimilating total columns, while the horizontal correlation depended only on the distance between the model grid cells. Here, we follow the approach described by Segers et al. (2005), by parameterising the model covariance into a time dependent standard deviation field and a constant correlation field. Each time step, the model's advection operator is applied to the standard deviation field. The error growth (i.e. the addition of \mathbf{Q} in equation (7)) is modelled by a simple mathematical function, more details can be found in section 5.2. The model covariance matrix can now be calculated according to:

$$\mathbf{P} = \mathbf{D}(\sigma) \mathbf{C}\mathbf{D}(\sigma) \quad (12)$$

with $\mathbf{D}(\sigma)$ a matrix with the values of the standard deviation σ on the diagonal and \mathbf{C} the correlation matrix. The correlation matrix is calculated differently than in Segers et al. (2005), more details can be found in section 5.3.

Unfortunately, the $\left(\mathbf{H}_i\mathbf{P}_i^f\mathbf{H}_i^T + \mathbf{R}_i\right)$ matrix in the Kalman filter (equation (10)) is badly conditioned, which makes the inversion sensitive to noise. Therefore, the eigenvalue decomposition of this matrix is calculated and the measurements are projected on the largest eigenvalues, which in total represent 98% of the original trace of the matrix.

For the numerical stability of the assimilation algorithm, the difference between the observation and the model should not be too large. A filter is implemented that rejects the observation when the absolute difference between the observation and the model forecast is larger than three times the square root of the sum of the variance of the observation and the variance of the

forecast:

$$\text{abs} \left(\mathbf{y}_i - H \left(\mathbf{x}_i^f \right) \right) \geq 3 \sqrt{\sigma_{y_i}^2 + \sigma_{x_i^f}^2} \quad (13)$$

with σ_y and σ_x^f the standard deviation of the observation \mathbf{y} and the forecast $H(\mathbf{x}^f)$ for layer i respectively. Note that this is done on a layer-by-layer basis, i.e. if in one layer the difference is too large, the whole observed profile is discarded.

- 5 Not all available ozone profiles can be assimilated into TM5 because the computational cost would be too high. [Averaging retrievals on the model grid \(sometimes called superobservations\) was not possible, because the assimilation algorithm described in this paper requires AKs and averaging AKs is not straightforward.](#) Therefore 1 out of 3 GOME-2 profiles and 1 out of 31 OMI profiles are used. These numbers are chosen such that more or less the same number of observations are assimilated for each instrument, taking into account the decrease in available pixels due to the row anomaly in OMI. For OMI, the outermost
10 pixels on each side of the swath are neglected, because of the large area of these pixels. Of the resulting retrievals, only cloud free scenes (cloud fraction ≤ 0.2) are assimilated in order to get the maximum amount of information from the troposphere.

5 Improvements of the assimilation algorithm

- The first version of our assimilation algorithm was described in Segers et al. (2005). They assimilated GOME ozone profiles for the year 2000. This dataset was extended to the period 1996–2001 by de Laat et al. (2009) who derived tropospheric ozone
15 for this period. The assimilated GOME observations in the previous algorithm version had a pixel size of 960×100 km, much larger than the pixels in the current research. Since 2009, the assimilation algorithm has been further developed and improved for use with GOME-2. The improved resolution of GOME-2 and OMI ozone profiles and improved retrievals offer new possibilities, but also require adaptations in the data assimilation. It is the first time that ozone profiles from two nadir looking instruments, GOME-2 and OMI, are assimilated simultaneously. This has resulted in a significant number of updates
20 and improvements to the assimilation algorithm compared to the version described in Segers et al. and de Laat et al. (2009), which are outlined in the following sections.

5.1 Observational error characterisation

- The covariance matrix of the observations that is used in the assimilation is composed of two components, the error on the spectral observations and the error of the a-priori information. Since the spectral errors affect the assimilation results, they are
25 first verified, using the following method.

For a given wavelength two adjacent detector pixels may have a radiance or reflectance difference that depends on the slope of the spectrum. Given enough samples, the standard deviation of the mean difference is a good indication of the noise at that particular wavelength. The relative difference D is calculated as:

$$D = \frac{F(\lambda_1) - F(\lambda_2)}{0.5 (F(\lambda_1) + F(\lambda_2))} \quad (14)$$

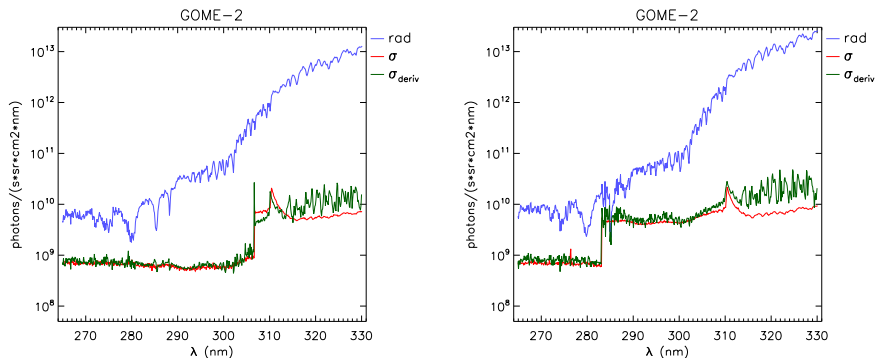


Figure 1. GOME-2 METOP-A radiance spectra calculated by OPERA: before (left) and after (right) the wavelength shift from 307 to 283 nm. The blue and red lines are the radiance and uncertainty that are used in OPERA. The green line shows the fitted standard deviations of the relative difference (see equation (14)) multiplied by the radiance.

where F is the radiance and λ_1 the wavelength in detector pixel 1 and λ_2 the wavelength in the adjacent pixel. Because the standard deviation is sensitive to outliers, a Gaussian distribution is fitted to the data. The fitted standard deviation is multiplied with the spectrum and compared to the reported noise in the level-1 data.

For GOME-2, we checked four days in 2008: 15 March, 25 June, 26 September and 25 December. On December 10th, 2008 the band 1A/B boundary was shifted from approximately 307 nm to 283 nm and the integration time ~~for band 1B in this wavelength range~~ decreased from 1.5s to 0.1875s ~~in this wavelength range~~ as was already the case for the rest of band 1B. Therefore, the data for the first three days are combined, while the data for 25 December is treated separately. The analysis was performed for different subsets, such as latitude, solar zenith angle and viewing angle, but results are shown for latitude only.

Figure 1 shows the resulting GOME-2 radiance spectra for all wavelengths. It should be noted that these results are made using spectral data derived with the GOME Data Processor (GDP) version 5.3. The older version GDP 4 uses a different noise model, which yielded too large errors.

The wavelength grid for OMI varies with the location across the detector, so the error verification has been performed with a dependence on the cross-track position. An example radiance spectrum along with the uncertainties is shown in the left panel of Figure 2. There is a jump in the spectral uncertainty (the red line) around 300 nm, which might be related to a change in the gain settings for the detector. For the selected pixel, the gain changes with a factor of 10 at 300nm.

On February 1, 2010, a L0 to L1b processor update was implemented for OMI. The new processor version includes more detailed information on the row anomaly and a new noise calculation for the three channels UV1, UV2 and VIS. More information can be found on the following website: http://projects.knmi.nl/omi/research/calibration/GDPS-History/GDPS_V113.html The new noise calculation was investigated by taking the radiance differences determined a few days after the update. The resulting radiance spectra are given in the right panel of Figure 2. The uncertainties in the L1 observations after the L0 to L1b processor update are about a factor of 5 smaller than the uncertainties derived according to the method described above.

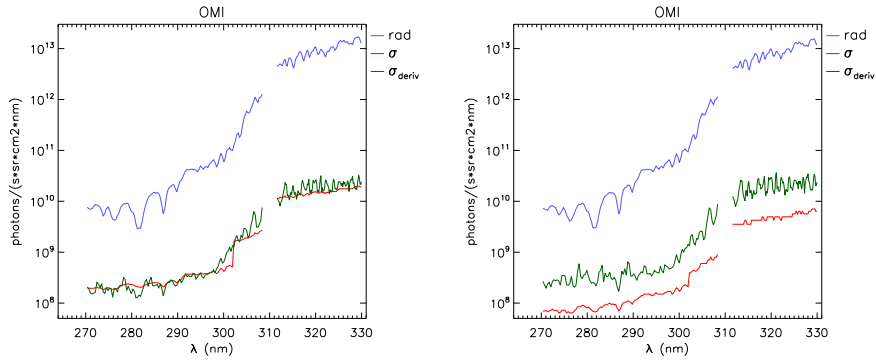


Figure 2. OMI radiance spectrum used in the retrieval, the area around 310 nm is not used. The blue and red lines are the radiance and uncertainty respectively. The green line shows the fitted standard deviations of the relative difference (see equation (14)) multiplied by the radiance. Left plot before the L0 to L1b processor update: date = 25-02-2006, lon = 145.2°, lat = -20.3°; right plot after the update: date = 5-2-2010, lon = 138.0°, lat = -28.0°.

In general, the spectral uncertainties for GOME-2 show a good agreement with our fitted uncertainties and therefore we simply use the uncertainties provided with the observations. The spectral uncertainties for OMI show a good agreement with our fitted uncertainties before the processor update, but are too small afterwards. The consequences of these smaller uncertainties will be shown in section 6. Since we use the OMI observations as they are, we are not able to correct for the spectral
5 uncertainties in the retrieval.

5.2 Model Error Growth

In section 4 we explained that using the full covariance propagation from the Kalman filter equations is too computational intensive, ~~instead~~. Instead we parameterise the model covariance matrix into a time dependent standard deviation field and a time independent correlation field. The advection operator is applied to the standard deviation field, and the model error growth
10 is modelled by applying a simple empirical relation.

In the previous version of the assimilation algorithm, the error growth for the total column was modelled by the function $e(t) = At^{1/3}$ (Eskes et al., 2003), with A a fit parameter. The error for the total column was distributed over the layers in the profile, proportional to the partial columns in each layer (Segers et al., 2005). Deriving a similar relation on a layer-by-layer basis was not successful, because the error can grow unlimited using this error growth description. Especially during the polar
15 night this might lead to unrealistic high error values.

Therefore, we use the following function

$$e(t) = \frac{at}{b+t} \quad (15)$$

where a and b are parameters which can be determined by fitting the observation minus forecast RMS as a function of time (see Eskes et al. (2003), figure 2). The parameter ~~a~~ a is the maximum ~~relative~~ error of the model at a particular altitude. At $t = b$,

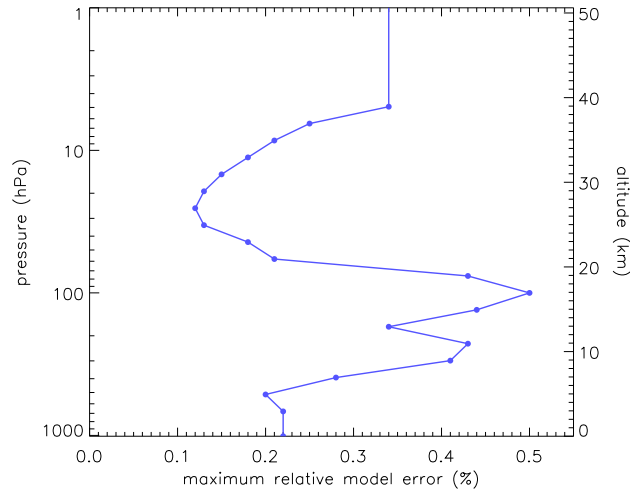


Figure 3. Values of Maximum relative model error (a) as a fraction of the partial column at different altitudes.

~~a a surface 0.22 131.50 0.44 19.38 0.13 678.57 0.22 100.03 0.50 14.74 0.15 516.19 0.20 76.09 0.43 11.21 0.18 392.68 0.28 57.88 0.21 8.53 0.21 298.72 0.41 44.03 0.18 6.49 0.25 227.24 0.43 33.50 0.13 4.94 0.34 172.86 0.34 25.48 0.12 TOA 0.34~~

the error is $0.5a$, therefore b is a measure of how fast the error grows after a measurement has been assimilated. The best results are obtained using $b = 2$ (days) and let the value of a vary over altitude. The values of a are determined by comparing the free model run (i.e. no assimilation) with all sondes for 2008. ~~These~~ Because the model currently runs on a $3^\circ \times 2^\circ$ (longitude \times latitude) grid and the sonde observations are essentially point sources, these results include a representation error due to the grid cell size of the model, and ~~The derived bias~~ is therefore an overestimation of the real model error. ~~Therefore, and to prevent the model error from increasing too rapidly~~ all collocations that are more than 3σ from the mean are discarded. The RMS values of the resulting collocations are used as values for a (see Table 1) for a , they are shown as relative values in Figure 3 for comparison over different altitudes. For the error of the layers above the maximum altitude of the sondes (about 5 hPa), a has been set to the same value as the last layer below the maximum altitude.

10 5.3 Model correlation matrix

In order to calculate the time independent correlation field, we follow the National Meteorological Center's method (NMC-method) to determine the correlation in the model (see Parrish and Derber, 1992; Segers et al., 2005). Segers et al. (2005) used a reference run based on 6-hourly meteorological forecasts as the starting point for forecast runs that last 9 days and start at 12 UTC. After a spin-up period, 9 forecast fields per day are available which can be used to determine the correlation in ozone.

15 Differences between the ozone concentration in these runs are due to the different meteorological inputs. Since the overpass frequency of GOME is three days, the forecast field from the run started 3 days before the current date was used to derive the correlations in the ozone field. This choice also best matched the correlation length found by Eskes et al. (2003), where total columns were assimilated instead of profiles.

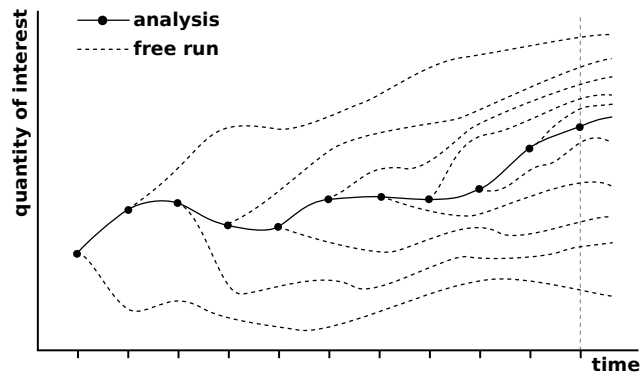


Figure 4. Determination of the TM5 correlation field. The solid line is an assimilation model run, the dashed lines are 10-day free model runs. After 10 days, there are 11 ozone fields for each given day which can be used to determine the correlations.

We use a slightly different approach as Segers et al. (2005) because their method neglects uncertainties due to the chemistry parameterisation. Also, the forecast lag of three days is not compatible with GOME-2 and OMI, which have daily global coverage. Our reference run is the result of the assimilation of profile observations for April 2008, which we consider the true state of the atmosphere. Using the analysis field at 0 UTC, a model run without assimilation (a free model run) is started for a duration of 10 days. After the first 10 days, there are 11 model fields for a given date at 12 UTC: 1 from the assimilation run and 10 from the free model runs (see Figure 4).

The difference between the assimilation and free model runs is used to determine the correlations between all pairs of grid cells in the vertical direction (constant location), in the East-West direction (constant latitude and altitude), and in the North-South direction (constant longitude and altitude). The correlations are determined as a function of the distance. Since the East-West distance between two grid cells is larger at the equator than near the poles, the East-West correlation also depends on the latitude. The calculated correlations as function of distance are fitted with a Gaussian distribution (with correlations less than 0.01 set to zero). Both the calculated and fitted correlations are shown in Figure 5. The fitted correlations are used in subsequent model runs as the time independent correlation field.

5.4 Ozone profile error characterisation and bias correction

The biases between two instruments should be as small as possible for a stable assimilation. Therefore, a bias correction as function of Solar Zenith Angle (SZA), Viewing Angle (VA) and time has been developed based on the results of the comparison with sondes. The bias correction factor is one minus the median of the relative deviation based on all collocated data in a given year. All observations in a given year are multiplied by this correction factor.

Figure 6 shows the [global](#) validation results for the four years of the assimilation period (2008–2011) of the GOME-2 and OMI profiles with ozone sondes downloaded from the World Ozone and Ultraviolet Radiation Data Center (WOUDC, WMO/GAW, 2016). [The validation methodology has been described in van Peet et al. \(2014\), and the main characteristics are the following. Only cloud free \(cloud fraction < 0.2\) retrievals have been used, the sonde launch location should be located in](#)

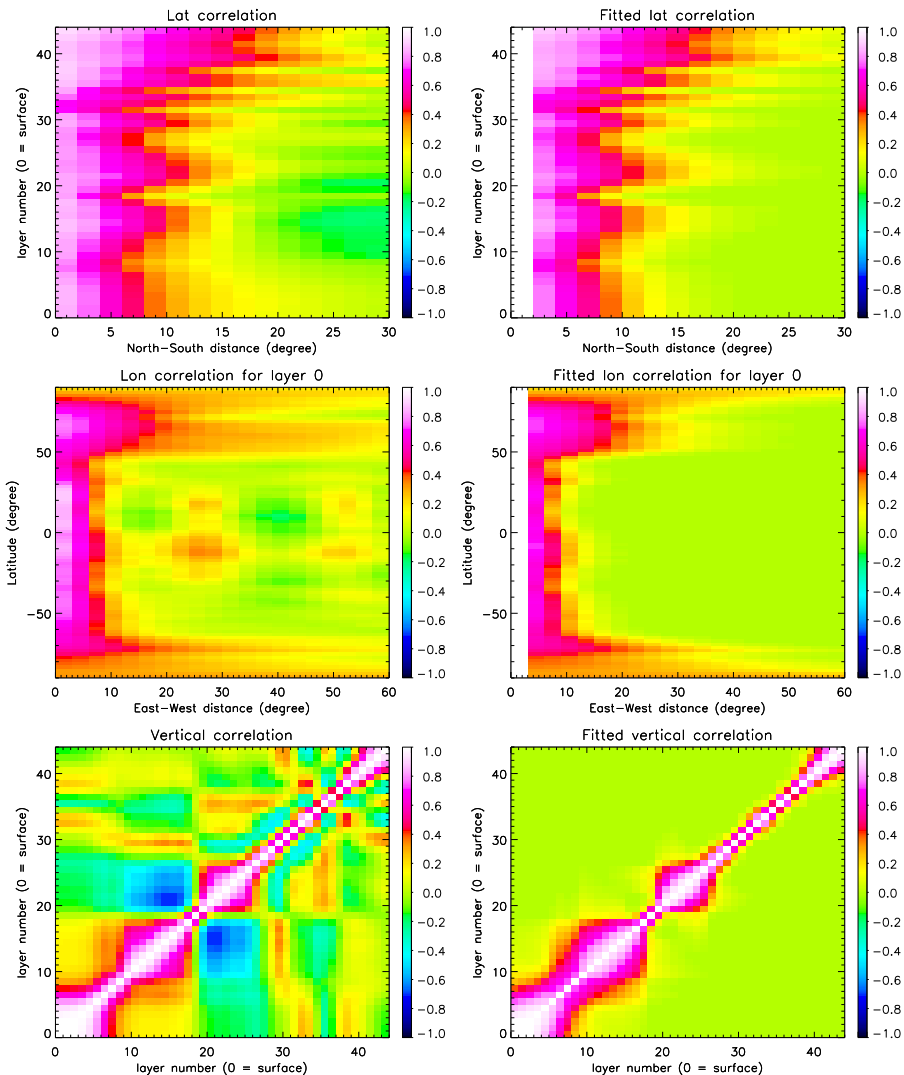


Figure 5. Calculated (left) and fitted (right) correlations for the latitudinal (top), surface layer longitudinal (middle) and vertical (bottom) directions.

the pixel footprint, and the satellite overpass time could be within 3 hours of sonde launch. When multiple retrievals collocate with the same sonde, only the one closest in time has been used. The collocated sonde profiles have been interpolated on the pressure grid of the retrievals and extended to the top of the atmosphere with the a-priori profile above the burst level of the sonde. The interpolated and extended profiles are convolved with the averaging kernels in order to take the vertical sensitivity

5 of the satellite instruments into account.

The bias of GOME-2 with respect to sondes varies between -1.1 and +1.7 DU (-7 and +7%) between 100 and 10 hPa, while for altitudes below 100 hPa the bias is about -0.3 DU (-4%). The bias of OMI varies between -4.5 and +2 DU (-8 and +15%)

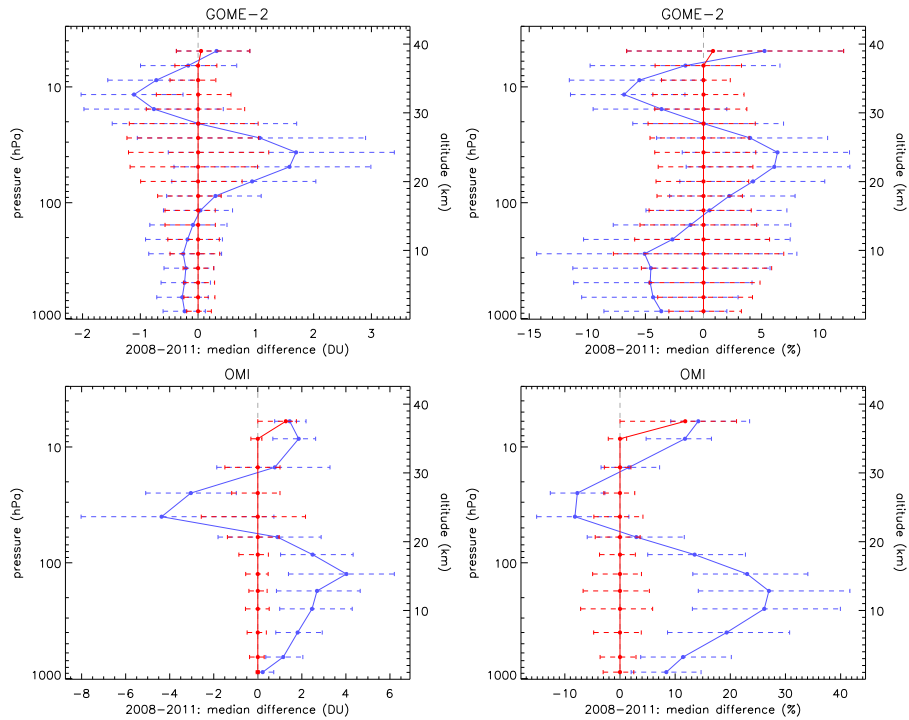


Figure 6. ~~Validation~~ Global validation results for 2008-2011 for GOME-2 at the top and OMI at the bottom. The left column shows the median absolute differences, the right column shows the median relative differences. The blue line indicates the original observations, the red line the bias corrected observations that have been used as input for the assimilation. The error bars indicate the range between the 25% and 75% percentiles. Note that the x-axis scale is different for each plot.

between 100 and 10 hPa, while below 10 hPa the bias is positive with a maximum value of 4 DU (+27%). The absolute biases cannot be compared directly because the layers of GOME-2 and OMI do not have the same thickness. Note that the remaining biases for the top layers in Figure 6 are not exactly zero for the corrected observations, because the figure is drawn for latitude bands, while the bias correction is made using SZA and VA bins and the number of sondes used in the comparison at that altitude is much smaller than at lower altitudes. ~~The~~ For the validation of GOME-2, 1083 sondes were used, of which 10 reached the top level. For the validation of OMI, 776 sondes were used of which 33 reached the top level. Table 1 lists all stations and the number of sondes in the lowest and top layers is 1083 and used in the validation and bias correction of the observations. The numbers in the station names refer to the WOUDC station identifiers.

Table 1. Stations used for the validation and bias correction of GOME-2 and OMI.

station	lon	lat	# GOME-2	# OMI
<u>stn_018_alert</u>	<u>-62.33</u>	<u>82.50</u>	<u>32</u>	<u>0</u>
<u>stn_021_edmonton-stony_plain</u>	<u>-114.11</u>	<u>53.55</u>	<u>0</u>	<u>4</u>
<u>stn_024_resolute</u>	<u>-94.97</u>	<u>74.71</u>	<u>27</u>	<u>1</u>
<u>stn_029_macquarie_island</u>	<u>158.94</u>	<u>-54.50</u>	<u>14</u>	<u>0</u>
<u>stn_043_lerwick</u>	<u>-1.19</u>	<u>60.14</u>	<u>31</u>	<u>26</u>
<u>stn_053_uccle</u>	<u>4.35</u>	<u>50.80</u>	<u>66</u>	<u>43</u>
<u>stn_055_vigna_di_valle</u>	<u>12.21</u>	<u>42.08</u>	<u>3</u>	<u>1</u>
<u>stn_076_goose_bay</u>	<u>-60.36</u>	<u>53.31</u>	<u>17</u>	<u>0</u>
<u>stn_089_ny_alesund</u>	<u>11.95</u>	<u>78.93</u>	<u>35</u>	<u>9</u>
<u>stn_101_syowa</u>	<u>39.58</u>	<u>-69.01</u>	<u>0</u>	<u>4</u>
<u>stn_107_wallops_island</u>	<u>-75.47</u>	<u>37.93</u>	<u>28</u>	<u>23</u>
<u>stn_109_hilo</u>	<u>-155.04</u>	<u>19.43</u>	<u>34</u>	<u>0</u>
<u>stn_156_payerne</u>	<u>6.57</u>	<u>46.49</u>	<u>153</u>	<u>156</u>
<u>stn_174_lindenberg</u>	<u>14.12</u>	<u>52.21</u>	<u>30</u>	<u>36</u>
<u>stn_175_nairobi</u>	<u>36.80</u>	<u>-1.27</u>	<u>25</u>	<u>10</u> respectively for GOME 2 and 776 and-
<u>stn_191_samoa</u>	<u>-170.56</u>	<u>-14.23</u>	<u>42</u>	<u>3</u>
<u>stn_199_barrow</u>	<u>-156.60</u>	<u>71.30</u>	<u>12</u>	<u>14</u>
<u>stn_219_natal</u>	<u>-35.26</u>	<u>-5.49</u>	<u>0</u>	<u>27</u>
<u>stn_221_legionowo</u>	<u>20.97</u>	<u>52.40</u>	<u>39</u>	<u>33</u> respectively for OMI-
<u>stn_233_marambio</u>	<u>-56.62</u>	<u>-64.24</u>	<u>23</u>	<u>2</u>
<u>stn_242_praha</u>	<u>14.44</u>	<u>50.00</u>	<u>29</u>	<u>48</u>
<u>stn_256_lauder</u>	<u>169.68</u>	<u>-45.04</u>	<u>4</u>	<u>7</u>
<u>stn_308_madrid-barajas</u>	<u>-3.58</u>	<u>40.47</u>	<u>59</u>	<u>52</u>
<u>stn_315_eureka-eureka_lab</u>	<u>-85.94</u>	<u>79.99</u>	<u>56</u>	<u>1</u>
<u>stn_316_debilt</u>	<u>5.18</u>	<u>52.10</u>	<u>40</u>	<u>29</u>
<u>stn_318_valentia_observatory</u>	<u>-10.25</u>	<u>51.93</u>	<u>37</u>	<u>19</u>
<u>stn_323_neumayer</u>	<u>-8.26</u>	<u>-70.65</u>	<u>63</u>	<u>11</u>
<u>stn_328_ascension_island</u>	<u>-14.42</u>	<u>-7.98</u>	<u>0</u>	<u>10</u>
<u>stn_330_hanoi</u>	<u>105.80</u>	<u>21.01</u>	<u>0</u>	<u>4</u>
<u>stn_336_isfahan</u>	<u>51.70</u>	<u>32.51</u>	<u>0</u>	<u>1</u>
<u>stn_338_bratts_lake-regina</u>	<u>-104.70</u>	<u>50.20</u>	<u>24</u>	<u>37</u>

continued on next page

station	lon	lat	# GOME-2	# OMI
stn_339_ushuaia	-68.31	-54.85	6	2
stn_344_hong_kong_observatory	114.17	22.31	4	28
stn_348_ankara	32.86	39.97	0	9
stn_394_broadmeadows	144.95	-37.69	36	29
stn_434_san_cristobal	-89.62	-0.92	1	0
stn_435_paramaribo	-55.21	5.81	33	0
stn_436_la_reunion_island	55.48	-21.06	20	11
stn_437_watukosek-java	112.60	-7.50	3	4
stn_438_suva_fiji	178.40	-18.13	6	3
stn_443_sepang_airport	101.70	2.73	6	0
stn_445_trinidad_head	-124.20	40.80	5	5
stn_450_davis	77.97	-68.58	5	12
stn_456_egbert	-79.78	44.23	22	13
stn_457_kelowna	-119.40	49.94	0	24
stn_466_maxaranguape-shadoz-nat	-35.26	-5.49	0	25
stn_477_heredia	-84.11	10.00	2	0
stn_494_alajuela	-84.21	9.98	11	0
	total		1083	776

6 Results and validation

We have assimilated GOME-2 (on Metop-A) and OMI ozone profiles for a period of 4 years between 2008-2011 using the Kalman filter algorithm described in the previous sections. In total, four model runs were performed: a 'free' model run without assimilation, a model run with assimilation of GOME-2 ozone profiles only, a model run with assimilation of OMI ozone profiles only and a model run with simultaneous assimilation of GOME-2 and OMI ozone profiles.

6.1 Altitude dependent OmF and OmA statistics

An important diagnostic of any assimilation system ~~are the differences~~ [is the difference](#) between the observations and the model (also known as innovations). In the following, we define the relative observation minus forecast (OmF) for layer i as:

$$10 \quad \text{OmF}_i = \frac{\mathbf{y}_i - H(\mathbf{x}_i^f)}{0.5(\mathbf{y}_i + H(\mathbf{x}_i^f))} \frac{|\mathbf{y}_i - H(\mathbf{x}_i^f)|}{0.5(\mathbf{y}_i + H(\mathbf{x}_i^f))} \quad (16)$$

with i the layer index, y the observed ozone profile, H the observation operator and x^f the forecast profile of the model (see section 4). The layers in the retrievals of GOME-2 and OMI have a different thickness, which makes the comparison of the OmF between the two instruments not straightforward. Therefore, both y and $H(x^f)$ have been regridded to the same pressure levels before calculating the OmF. This new ~~pressure-vertical~~ grid is defined by levels at 0, 6 and 12 km followed by levels every 2 km up to 60 km, ~~corresponding to~~ which are converted to hPa and correspond to surface pressure up to 0.28 hPa. The observation minus analysis (OmA) is defined in a similar way, but with x^f replaced with the analysis profile x^a . Since the analysis field is a weighted average of the forecast model field and the observations, the OmA should be smaller than the OmF.

In Figure 7, the GOME-2 OmF and OmA from the model run with simultaneous assimilation of GOME-2 and OMI for four different layers have been plotted. The ozone sondes that were used in deriving the bias correction and the validation of the results were required to have reached at least 10 hPa. Therefore the selected layers in Figure 7 are the surface layer, the layer just below and above 10 hPa, and the top layer of the new pressure grid around 60 km (0.3 hPa). In Figure 8, the OmF and OmA for the same layers have been plotted for OMI. In the first year of the assimilation period, the surface layer OmF and OmA for GOME-2 are higher than those for OMI. At the end of 2008, after the wavelength shift between GOME-2 band 1A/1B, the situation is reversed and the OmF and OmA for GOME-2 are lower than those for OMI. The band 1A/1B wavelength shift is clearly present in the bottom layer of the GOME-2 OmF and OmA, which might be unexpected since the radiation from band 1A/1B does not reach the surface. But since the layers in an optimal estimation retrieval are related as described by the AK and covariance matrices, it is possible that the band 1A/1B change affects the results in an altitude region where the radiation itself does not penetrate. The OMI data show a more pronounced yearly cycle than GOME-2. After the beginning of 2010, the OmF and OmA for both instruments are very similar for the summer months June, July and August, but the winter time values for OMI are higher. For the layer just below the 10 hPa, the OmF and OmA for GOME-2 are about 1 percent point higher than for OMI. For the layer just above the 10 hPa, the OmF and OmA for GOME-2 start out lower than for OMI, but at the end of the assimilation period, the values are comparable. For the top layer, the OmF and OmA for GOME-2 are about 5 percent point higher than for OMI. In general, the OmF is about 2–4 percent point higher than the OmA, except for the top layer. There, the difference is in the order of 1 percent point, but the values vary much more than lower in the atmosphere.

Both OmF and OmA for the GOME-2 assimilation run show regular decreases with a period of about one month. These decreases are caused by GOME-2 being operated in 'narrow-swath mode', when the swath is 320 km wide instead of 1920 km. For these narrow-swath observations, the model is closer to the retrieved profiles, causing a lower OmF/OmA. OMI also has a spatial zoom-in mode, which is activated about once a month, but these pixels are filtered out because they are too much influenced by the row-anomaly and because the mapping between the UV-1 and UV-2 pixels changes with respect to the normal mode. Peaks in the OmF and OmA for the GOME-2 assimilation, such as after an instrument test period between 7 and 12 September 2009, can be related to periods of missing data.

Sudden changes in the OmF and OmA are visible for some altitudes for both instruments at the start of some years. One example is in the layer just above the 10 hPa for GOME-2 at the start of 2009 or at the start of 2010 for OMI. The change for GOME-2 appears to coincide with the band 1A/1B shift, but it is really at the start of the year and not on December 10th, 2008.

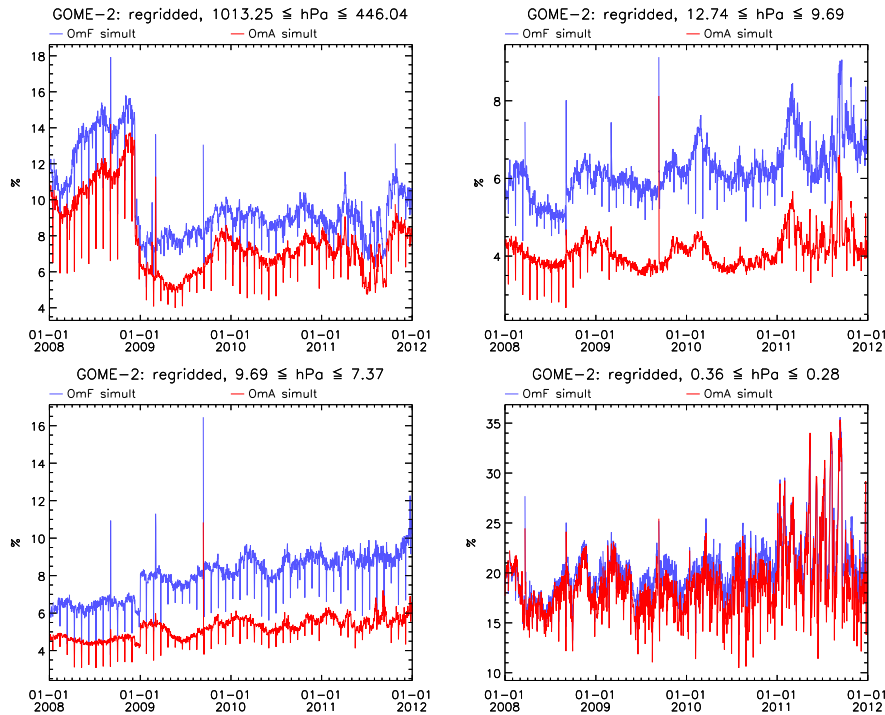


Figure 7. GOME-2 OmF (blue) and OmA (red) for the surface layer (top left), around 10 hPa (top right and bottom left) and around 0.3 hPa (bottom right). The OmF and OmA have been calculated for the regridded layers from the model run with simultaneous assimilation of GOME-2 and OMI.

It is therefore unlikely that these two events are related. Since there are no known instrumental or meteorological changes, the most likely cause is therefore the bias correction scheme for the observations, which changes its correction parameters at the start of each year.

5 Closer inspection of the OMI OmF and OmA change at the start of 2010 (see the lower left panel of Figure 8, shows that it actually consists of two steps: the first one at the start of the year, and the second one a month later. That second step is also present in the lower right panel (the layer around 0.3 hPa), where the change is about 5 percent point, but it is less clear due to the higher variability in the signal. Figure 9 shows the same data, but focused on the first two months of 2010. Both OmF and OmA increase by about 5 percent point from one day to the next. The increase is even larger (and more clearly visible) in the data from the single instrument assimilation run for OMI.

10 Comparison of Figure 7 and Figure 8 shows that the OmF and OmA for one instrument might be larger than for the other, depending on the altitude. Which of the two instruments has a larger OmF or OmA value might also change over time. In other words, GOME-2 and OMI have a different sensitivity for different altitudes as represented by the averaging kernels. Assimilating the observations from these instruments simultaneously, increases the overall sensitivity of the assimilation.

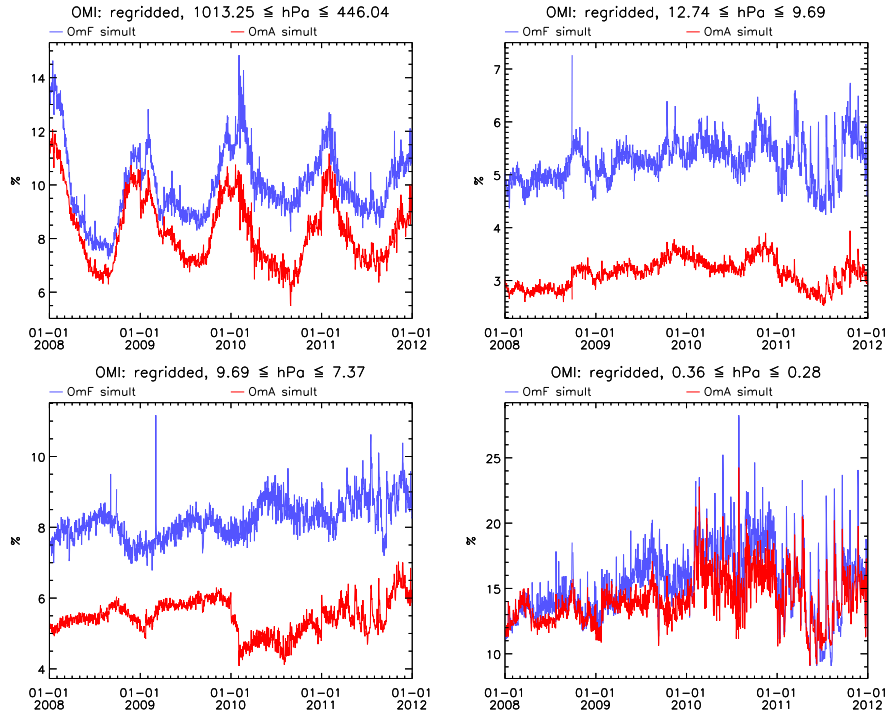


Figure 8. OMI OmF (blue) and OmA (red) for the surface layer (top left), around 10 hPa (top right and bottom left) and around 0.3 hPa (bottom right). The OmF and OmA have been calculated for the regridded layers from the model run with simultaneous assimilation of GOME-2 and OMI.

Lower uncertainties in the spectra lead to lower uncertainties on the observations, which on its turn changes the balance between model and observations in the Kalman filter and affects the innovations. Because the variance of the observation is lower, more pixels will be rejected by the OmF filter (see section 4 and Figure 10). The figure shows the number of assimilated observations for both GOME-2 and OMI from the single and simultaneous instrument assimilation. In the single instrument
 5 assimilation runs, the model error is adapted to the new situation after the processor update and the total number of assimilated observations does not change. For the simultaneous assimilation, the ~~OmF differences become so large with respect to the uncertainties, that assimilation results may be fluctuating between OMI and GOME-2 observations if a bias exists. This might result in higher assimilation errors. Therefore,~~ the OmF filter (see section 4, equation 13) rejects observations from both GOME-2 and OMI, even though only the ~~OMI data uncertainties from one of the instruments (i.e. OMI)~~ have changed.

10 6.2 Altitude independent OmF and OmA statistics

In order to show the geographical distribution of the OmF and OmA, the absolute values for each layer were quadratically added and the square root was taken from the result. These column integrated OmF and OmA values were averaged on a daily

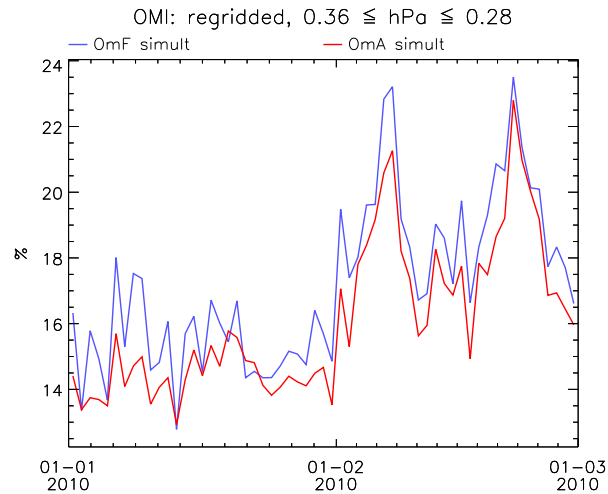


Figure 9. OMI OmF (blue) and OmA (red) for the layer around 0.3 hPa, zoomed in to a month before and after the L0 to L1b processor update. The OmF and OmA have been calculated for the regridded layers from the model run with simultaneous assimilation of GOME-2 and OMI.

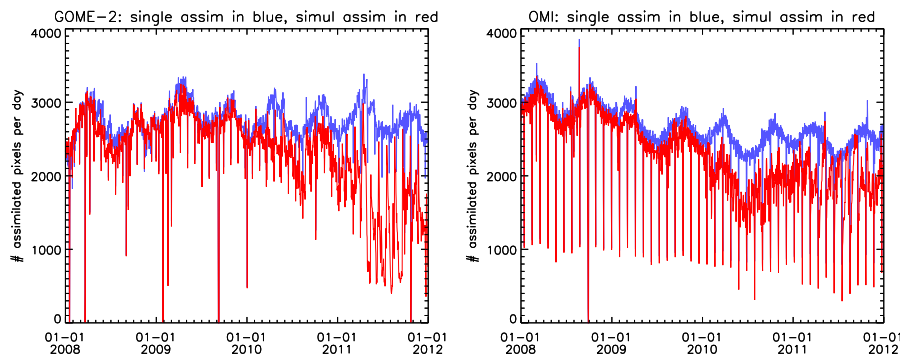


Figure 10. Number of assimilated observations from GOME-2 (left) and OMI (right). The blue lines represent the single instrument assimilation, the red lines the simultaneous assimilation.

basis for latitude bins with a size of 2° . In Figure 11 these column integrated OmF and OmA are shown as function of latitude and time.

The highest values of the OmF and OmA are observed at high latitudes around the polar night. The ~~wavelength change in Band 1B Gome-2 band 1A/1B wavelength change~~ is clearly visible ~~for the GOME-2 data. Another step change, even though~~ the plot shows OmF and OmA from the combined assimilation. Step changes in the OmA ~~is visible for both the GOME-2 and OMI assimilation runs are visible~~ at the start of 2011 each year, which coincides with an update of the bias correction parameters. ~~OMI data is missing at latitudes larger than 80 degrees for 2009 onward due to the row anomaly.~~

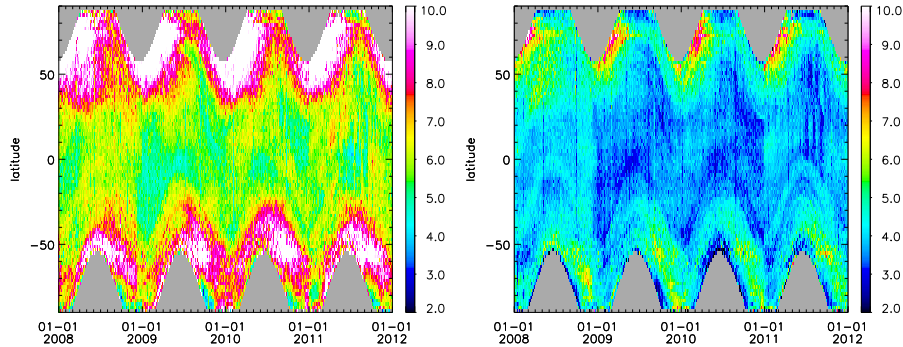


Figure 11. Mean OmF (left column) and OmA (right column) as a function of latitude (binsize 2°) and time (binsize 1 day) for the simultaneous assimilation of GOME-2 and OMI.

6.3 Expected and observed OmF

The OmF of the results should be consistent with the uncertainties of the observations and the model forecast. The expected OmF is based on the observation error and the forecast error and is the mean of the square root term in the right hand side of equation (13) for all observations in a given layer. The observed OmF for each layer for the whole assimilation period on the other hand is the mean of the left hand side of equation (13). In Figure 12, the observed OmF is plotted as a function of the expected OmF for the model runs with assimilation of GOME-2 only, with assimilation of OMI only, and for both instruments separate with the data taken from the model run with simultaneous assimilation.

Note that the pressure levels are those from the observations, not the regridded levels used in the calculation of the OmF and OmA above. The expected and observed OmF are close to the 1-to-1 line, which shows that the model error $\sigma_{\omega f}$ is of the correct magnitude for the current observations. The expected and observed OmF are somewhat closer to the 1-to-1 line in the case of the simultaneous assimilation of GOME-2 and OMI than for the assimilation of each instrument independently. The model error that is used is therefore probably slightly better suited for the assimilation of multiple instruments simultaneously than for the assimilation of a single sensor.

6.4 Assimilation validation with sondes

The model output was validated against ozone sondes that were obtained from the World Ozone and Ultraviolet Radiation Data Center (WOUDC, WMO/GAW, 2016), see Figure 13. This is the same ozone dataset as was used to derive the bias correction. Note however that many more observations are assimilated than were used deriving the bias correction, while all observations are corrected with the same factor. The assimilation model runs are significantly better than the free model run. This is especially true for the part of the atmosphere where GOME-2 and OMI are most sensitive to the ozone concentration, between 100 and 10 hPa. In this area, the model run with assimilation of GOME-2 only shows a negative bias with respect to the ozone sondes, while the assimilation of OMI shows a positive bias. The assimilation of both GOME-2 and OMI shows

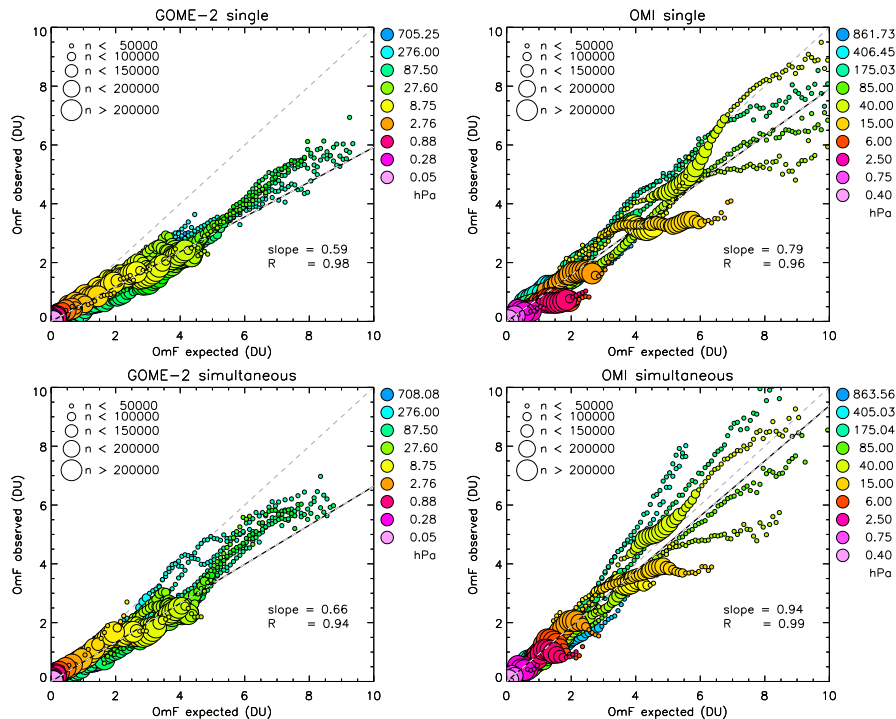


Figure 12. Observed vs. expected OmF. Top left: assimilation of GOME-2 only, top right: assimilation of OMI only. Bottom row: results from the simultaneous assimilation of both GOME-2 and OMI. Bottom left: GOME-2, bottom right: OMI. Colors indicate the pressure levels. Note that not all levels are plotted in the legend while all levels are plotted in the figure. The size of the circles gives the number of assimilated pixels (n) in that respective OmF-bin (bin-size = 0.2 DU). The slope for the fitted (dashed) line is given in the lower right corner of each panel, as is the correlation (R) between the expected and observed OmF.

the smallest bias. The deviation in the differences are very similar for the four runs, which is why only the error bars for the simultaneous assimilation have been plotted in Figure 13. The 25-75 percentile differences are in the 20-55 %-points range between 0 and 20 km and in the 10-20 %-points range between 20 and 40 km.

In the troposphere the assimilation also improves, but not as much as in the stratosphere. Note that in the troposphere the chemistry scheme is different than in the stratosphere (see section 3). The assimilation shows a deviation in the tropopause, between 200 and 100 hPa, although the L2 data does not show such large biases (see Figure 6). The vertical resolution of model and observation is different, therefore the ozone from the observation has to be redistributed over the model layers, a process which is included in the operator H . A small error in the redistribution of ozone in a region with a strong gradient in the concentration (such as the tropopause) will result in large uncertainties in the ozone concentration at this altitude. Above 10 hPa the assimilation shows increasing biases, and the difference with the free model run decreases. Although the L2 data also shows an increasing bias above 10 hPa, it should be noted that the number of sondes reaching this altitude is limited with respect to the tropopause region between 200 and 100 hPa. Also, there is a representation error of the sonde with respect to

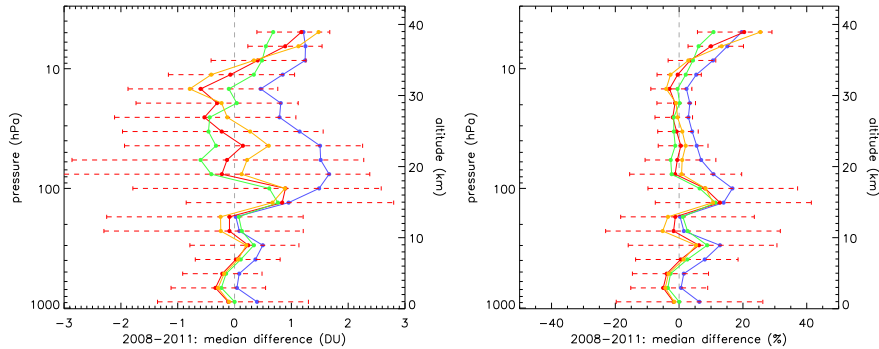


Figure 13. Validation of the model runs [with ozone sondes](#) for 2008-2011. Left: the median of the absolute difference in DU, right: the median of the relative differences. Blue: model run without assimilation, green: model run with assimilation of GOME-2 only, yellow: run with assimilation of OMI only, red: assimilation of both GOME-2 and OMI. The error bars are plotted for the simultaneous assimilation only, and range from the 25% to the 75% percentile.

the 3° longitude $\times 2^\circ$ latitude model grid. Therefore it is not as straightforward to attribute this increase in bias to either model or observation error.

7 Case study

To demonstrate the performance of the assimilation algorithm we analysed the results for a day above the Tibetan Plateau (located between 30°N and 40°N), where a highly dynamical atmosphere exists. [This makes it an interesting area to study atmospheric dynamics, and difficult for modelling so it can serve as a test case to see if the dynamics in the model are correctly implemented. On February 25th, 2008 a stratosphere-troposphere exchange event was observed in GOME-2 data \(Chen et al., 2013\), which can also be observed in the assimilation output.](#) In Figure 14, ozone concentrations from the ERA-Interim reanalysis (Dee et al., 2011; Dragani, 2011) are plotted as contours over the ozone concentrations from the model runs with and without simultaneous assimilation of GOME-2 and OMI. There is a significantly better agreement between the two datasets north of 35°N at pressure levels between 70 and 10 hPa. Even though the GOME-2 and OMI instruments have limited sensitivity in the troposphere, the tropospheric ozone concentrations of the ERA-Interim reanalysis and assimilated tropospheric ozone are in better agreement north of the Tibetan Plateau. There are also two stratosphere-troposphere exchanges (STE) visible, at 30°N and 60°N . These STEs are associated with strong jet-streams (perpendicular to the page) reaching wind speeds of up to 50 m/s at 250 hPa.

8 Discussion

When two instruments are assimilated simultaneously, their differences should be taken into account. For example, the algorithms used for the retrieval of GOME-2 and OMI ozone profiles both produce partial columns. However, the number of

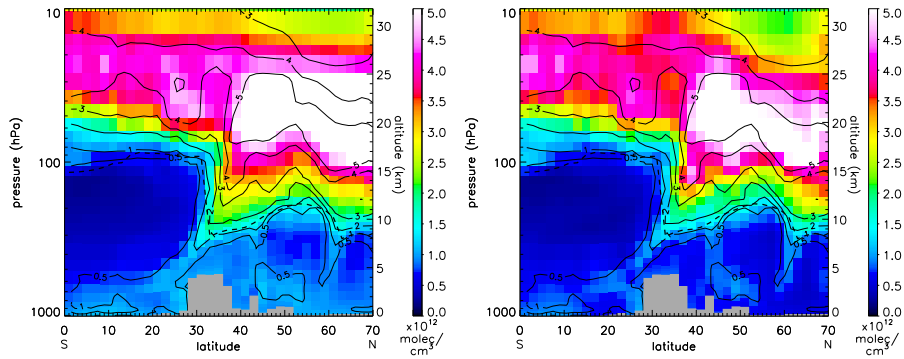


Figure 14. Two meridional cross sections over the Tibetan Plateau, located at 84.25°E on 25-02-2008, 6 UTC. The colors indicate the ozone concentration from the free model run (left) and the assimilation of both GOME-2 and OMI (right). The solid contours show the ozone concentrations from the ERA-Interim reanalysis. The dashed line shows the thermal tropopause.

layers in the retrievals differ and the sensitivity of the retrieval is expressed by the averaging kernel. Both the different vertical resolution and the averaging kernel are incorporated into the observation operator H . Both instruments have different horizontal resolution, something which has not been taken into account in the current version of the assimilation algorithm. The measurement principle of GOME-2 (i.e. a cross-track scanning mirror) is different than that of OMI (i.e. a fixed 2D CCD detector). As a result, the ground pixel size of GOME-2 is constant, while that of OMI varies across the track. Therefore, the representation error of OMI will increase towards the edges of the swath. The effect of the changing OMI footprint size has not been investigated. [To get an idea of the sub-gridcell variation of the ozone concentration, we performed a small experiment where we assimilated the same observations \(i.e. GOME-2 and OMI\) into TM5 running on a \$1^{\circ} \times 1^{\circ}\$ grid \(as opposed to the standard \$3^{\circ} \times 2^{\circ}\$ used in this article\). The total column standard deviation of the six \$1^{\circ} \times 1^{\circ}\$ gridcells covered by a single \$3^{\circ} \times 2^{\circ}\$ gridcell is much smaller than the error on the total column. Therefore, the representation error due to the large gridcells is not significant.](#) A more thorough check on the instruments behaviour throughout time might have revealed the effect of the OMI L0 to L1b processor update sooner. The threshold of the parameter in the OmF filter might be made instrument and time dependent in order to minimise the effect on the number of assimilated pixels.

Two different instruments can be biased with respect to each other. In order to minimise the bias, a bias correction scheme has been implemented with respect to ozone sondes. We used cloud free observations (max. cloud fraction 0.20) for the bias correction in order to get a maximum amount of information from the troposphere. As a consequence, we could not use all available sondes in deriving the bias correction. Sudden changes in the bias correction parameters are visible at the start of the year, when the parameters are changed. To minimise these changes, it might be worthwhile to implement an interpolation scheme for the bias correction parameters similar as for the MSR data (see van der A et al., 2010, 2015).

The model can run a full chemistry scheme, but instead a parameterised chemistry scheme has been used in favour of speed. Another possibility to increase the accuracy of the model is to increase the horizontal resolution from the current $3^{\circ} \times 2^{\circ}$ (lon

× lat) to for example $1^\circ \times 1^\circ$. However, in both cases it might be necessary to reduce the vertical resolution of the model to keep the computational cost at an acceptable level.

The model covariance matrix is also an expensive step in the assimilation algorithm. We have reduced the calculation cost by parameterising it into a time dependent error field and a time independent correlation field. The data from April 2008 was used to derive the correlations, which were then used for the whole assimilation period. The assumption that the derived correlations are constant throughout time has not been tested ~~due to lack of time and resources.~~

9 Conclusions

An algorithm for the simultaneous assimilation of GOME-2 and OMI ozone profiles has been described. The algorithm uses a Kalman filter to assimilate the ozone profiles into the TM5 chemical transport model. Compared to previous versions, the algorithm is significantly updated. The observational error has been characterised using a newly developed in-flight calibration method. Since the Kalman filter equations are too expensive to calculate directly for the current setup, the model covariance matrix is divided into a time dependent error field and a time independent correlation field. The time evolution is applied to the error field only, while the correlation is assumed to be constant. The model error growth is modelled by a new function that prevents the error from increasing indefinitely, and the correlation field has been newly derived using the NMC method. Large biases between retrievals of the two instruments might destabilise the assimilation. To avoid this, a bias correction using global ozone sonde observations has been applied to the retrieved ozone profiles before assimilation.

Four model runs were performed spanning the years between 2008 and 2011: without assimilation, with assimilation of GOME-2 only, with assimilation of OMI profiles only and with simultaneous assimilation of both GOME-2 and OMI profiles. Depending on the altitude, the OmF and OmA for one instrument might be larger than the other, which might change in the course of time. Assimilating the observations from these instruments simultaneously, increases the overall sensitivity of the assimilation. Two notable instrumental effects are the band 1A/1B wavelength shift for GOME-2, which causes a significant decrease in OmF and OmA. For OMI, after the L0 to L1b processor update on 1-2-2010, the uncertainty in the observations is too small with respect to the method of in-flight validation of the uncertainties presented in this paper. This caused a decrease in the number of assimilated observations for both GOME-2 and OMI. ~~The OmF and OmA of the simultaneous assimilation of both instruments is between the values of the single sensor assimilation. The~~ expected and observed OmF and OmA are more similar for the combined assimilation than for the separate assimilation. Validation with sondes from the WOUDC shows that the combined assimilation performs better than the single sensor assimilation in the region between 100 and 10 hPa where GOME-2 and OMI are most sensitive. The ozone concentrations in the troposphere are also affected by the assimilation, even though the instruments have limited sensitivity in that region. The biases of the assimilated ozone fields are smaller than those of the observations. The assimilated ozone fields are produced at regular time intervals and have no missing data. Despite the limited vertical resolution of GOME-2 and OMI, a case study of an STE over the Tibetan plateau shows that the assimilation of ozone profiles can improve the ozone distribution in a highly dynamical region.

Competing interests. The authors declare that they have no conflict of interest.

Acknowledgements. The authors acknowledge all scientists and institutes who contributed their ozone sonde data to the World Ozone and Ultraviolet Radiation Data Center (WOUDC, WMO/GAW, 2016), and the Meteorological Service of Canada for hosting this important public database. The authors would also like to thank Pepijn Veeffkind for his comments in preparation of this paper. EUMETSAT is acknowledged
5 for providing the GOME-2 L1 data and Olaf Tuinder and Robert van Versendaal for their help in the retrieval of the GOME-2 ozone profiles. The Dutch-Finnish OMI instrument is part of the NASA EOS Aura satellite payload. The OMI ozone profiles (OMO3PR, v003) were retrieved at NASA Goddard Earth Sciences Data and Information Services Center (GES DISC) and accessed from the local storage at the Royal Netherlands Meteorological Institute (KNMI). [Part of this research has been funded by the Ozone_cci project \(http://www.esa-ozone-cci.org\), which is part of the Climate Change Initiative \(CCI\) program of the European Space Agency \(ESA\).](http://www.esa-ozone-cci.org)

References

- Bhartia, P. K., McPeters, R. D., Flynn, L. E., Taylor, S., Kramarova, N. A., Frith, S., Fisher, B., and DeLand, M.: Solar Backscatter UV (SBUV) total ozone and profile algorithm, *Atmospheric Measurement Techniques*, 6, 2533–2548, <https://doi.org/10.5194/amt-6-2533-2013>, 2013.
- 5 Bovensmann, H., Burrows, J. P., Buchwitz, M., Frerick, J., Noël, S., Rozanov, V. V., K. V. Chance, and Goede, A. P. H.: SCIAMACHY: Mission Objectives and Measurement Modes, *Journal of Atmospheric Sciences*, 56, 127–150, [https://doi.org/10.1175/1520-0469\(1999\)056<0127:SMOAMM>2.0.CO;2](https://doi.org/10.1175/1520-0469(1999)056<0127:SMOAMM>2.0.CO;2), 1999.
- Burrows, J. P., Weber, M., Buchwitz, M., Rozanov, V., Ladstätter-Weissenmayer, A., Richter, A., Debeek, R., Hoogen, R., Bramstedt, K., Eichmann, K.-U., Eisinger, M., and Perner, D.: The Global Ozone Monitoring Experiment (GOME): Mission Concept and First Scientific
- 10 Results., *Journal of Atmospheric Sciences*, 56, 151–175, [https://doi.org/10.1175/1520-0469\(1999\)056<0151:TGOMEG>2.0.CO;2](https://doi.org/10.1175/1520-0469(1999)056<0151:TGOMEG>2.0.CO;2), 1999.
- Callies, J., Corpaccioli, E., Eisinger, M., Hahne, A., and Lefebvre, A.: GOME-2 – Metop’s Second-Generation Sensor for Operational Ozone Monitoring, *ESA bulletin*, 102, 28–36, 2000.
- Cariolle, D. and Teyssèdre, H.: A revised linear ozone photochemistry parameterization for use in transport and general circulation models: multi-annual simulations, *Atmospheric Chemistry and Physics*, 7, 2183–2196, 2007.
- 15 Chen, X., Añel, J. A., Su, Z., de la Torre, L., Kelder, H., van Peet, J., and Ma, Y.: The Deep Atmospheric Boundary Layer and Its Significance to the Stratosphere and Troposphere Exchange over the Tibetan Plateau, *PLoS ONE*, 8, e56909, <https://doi.org/10.1371/journal.pone.0056909>, 2013.
- de Laat, A. T. J., van der A, R. J., and van Weele, M.: Evaluation of tropospheric ozone columns derived from assimilated GOME ozone profile observations, *Atmospheric Chemistry and Physics*, 9, 8105–8120, 2009.
- 20 Dee, D. P., Uppala, S. M., Simmons, A. J., Berrisford, P., Poli, P., Kobayashi, S., Andrae, U., Balmaseda, M. A., Balsamo, G., Bauer, P., Bechtold, P., Beljaars, A. C. M., van de Berg, L., Bidlot, J., Bormann, N., Delsol, C., Dragani, R., Fuentes, M., Geer, A. J., Haimberger, L., Healy, S. B., Hersbach, H., Hólm, E. V., Isaksen, L., Kållberg, P., Köhler, M., Matricardi, M., McNally, A. P., Monge-Sanz, B. M., Morcrette, J.-J., Park, B.-K., Peubey, C., de Rosnay, P., Tavolato, C., Thépaut, J.-N., and Vitart, F.: The ERA-Interim reanalysis: configuration and performance of the data assimilation system, *Quarterly Journal of the Royal Meteorological Society*, 137, 553–597,
- 25 <https://doi.org/10.1002/qj.828>, 2011.
- Dethof, A. and Hólm, E. V.: Ozone assimilation in the ERA-40 reanalysis project, *Quarterly Journal of the Royal Meteorological Society*, 130, 2851–2872, <https://doi.org/10.1256/qj.03.196>, 2004.
- Dragani, R.: On the quality of the ERA-Interim ozone reanalyses: comparisons with satellite data, *Quarterly Journal of the Royal Meteorological Society*, 137, 1312–1326, <https://doi.org/10.1002/qj.821>, 2011.
- 30 Errera, Q., Daerden, F., Chabrilat, S., Lambert, J. C., Lahoz, W. A., Viscardy, S., Bonjean, S., and Fonteyn, D.: 4D-Var assimilation of MIPAS chemical observations: ozone and nitrogen dioxide analyses, *Atmospheric Chemistry and Physics*, 8, 6169–6187, 2008.
- Eskes, H. J., Velthoven, P. F. J. V., Valks, P. J. M., and Kelder, H. M.: Assimilation of GOME total-ozone satellite observations in a three-dimensional tracer-transport model, *Quarterly Journal of the Royal Meteorological Society*, 129, 1663–1681, <https://doi.org/10.1256/qj.02.14>, 2003.
- 35 Evensen, G.: The Ensemble Kalman Filter: theoretical formulation and practical implementation, *Ocean Dynamics*, 53, 343–367, <https://doi.org/10.1007/s10236-003-0036-9>, 2003.

- Flemming, J., Huijnen, V., Arteta, J., Bechtold, P., Beljaars, A., Blechschmidt, A.-M., Diamantakis, M., Engelen, R. J., Gaudel, A., Inness, A., Jones, L., Josse, B., Katragkou, E., Marecal, V., Peuch, V.-H., Richter, A., Schultz, M. G., Stein, O., and Tsikerdekis, A.: Tropospheric chemistry in the Integrated Forecasting System of ECMWF, *Geoscientific Model Development*, 8, 975–1003, <https://doi.org/10.5194/gmd-8-975-2015>, 2015.
- 5 Fortuin, J. P. F. and Kelder, H.: An ozone climatology based on ozonesonde and satellite measurements, *Journal of Geophysical Research*, 103, 31 709–31 734, <https://doi.org/10.1029/1998JD200008>, 1998.
- Hoogen, R., Rozanov, V. V., and Burrows, J. P.: Ozone profiles from GOME satellite data: Algorithm description and first validation, *Journal of Geophysical Research*, 104, 8263–8280, <https://doi.org/10.1029/1998JD100093>, 1999.
- Houtekamer, P. L. and Zhang, F.: Review of the Ensemble Kalman Filter for Atmospheric Data Assimilation, *Monthly Weather Review*, 144, 4489–4532, <https://doi.org/10.1175/MWR-D-15-0440.1>, 2016.
- 10 Huijnen, V., Williams, J., van Weele, M., van Noije, T., Krol, M., Dentener, F., Segers, A., Houweling, S., Peters, W., de Laat, J., Boersma, F., Bergamaschi, P., van Velthoven, P., Le Sager, P., Eskes, H., Alkemade, F., Scheele, R., Nédélec, P., and Pätz, H.-W.: The global chemistry transport model TM5: description and evaluation of the tropospheric chemistry version 3.0, *Geoscientific Model Development*, 3, 445–473, <https://doi.org/10.5194/gmd-3-445-2010>, 2010.
- 15 Huijnen, V., Flemming, J., Chabrillat, S., Errera, Q., Christophe, Y., Blechschmidt, A.-M., Richter, A., and Eskes, H.: C-IFS-CB05-BASCOE: stratospheric chemistry in the Integrated Forecasting System of ECMWF, *Geoscientific Model Development*, 9, 3071–3091, <https://doi.org/10.5194/gmd-9-3071-2016>, 2016.
- Krol, M., Houweling, S., Bregman, B., van den Broek, M., Segers, A., van Velthoven, P., Peters, W., Dentener, F., and Bergamaschi, P.: The two-way nested global chemistry-transport zoom model TM5: algorithm and applications, *Atmospheric Chemistry and Physics*, 5, 417–432, <https://doi.org/10.5194/acp-5-417-2005>, 2005.
- 20 Kroon, M., de Haan, J. F., Veefkind, J. P., Froidevaux, L., Wang, R., Kivi, R., and Hakkarainen, J. J.: Validation of Operational Ozone Profiles from the Ozone Monitoring Instrument, *Journal of Geophysical Research (Atmospheres)*, 116, <https://doi.org/10.1029/2010JD015100>, 2011.
- Lefever, K., van der A, R., Baier, F., Christophe, Y., Errera, Q., Eskes, H., Flemming, J., Inness, A., Jones, L., Lambert, J.-C., Langerock, B., Schultz, M. G., Stein, O., Wagner, A., and Chabrillat, S.: Copernicus stratospheric ozone service, 2009–2012: validation, system inter-comparison and roles of input data sets, *Atmospheric Chemistry and Physics*, 15, 2269–2293, <https://doi.org/10.5194/acp-15-2269-2015>, 2015.
- 25 Lerot, C., Van Roozendaal, M., Spurr, R., Loyola, D., Coldewey-Egbers, M., Kochenova, S., van Gent, J., Koukouli, M., Balis, D., Lambert, J.-C., Granville, J., and Zehner, C.: Homogenized total ozone data records from the European sensors GOME/ERS-2, SCIAMACHY/Envisat, and GOME-2/MetOp-A, *Journal of Geophysical Research (Atmospheres)*, 119, 1639–1662, <https://doi.org/10.1002/2013JD020831>, 2014.
- 30 Levelt, P. F., van den Oord, G. H. J., Dobber, M. R., Malkki, A., Visser, H., de Vries, J., Stammes, P., Lundell, J. O. V., and Saari, H.: The Ozone Monitoring Instrument, *IEEE Transactions on Geoscience and Remote Sensing*, 44, 1093–1101, <https://doi.org/10.1109/TGRS.2006.872333>, 2006.
- 35 Migliorini, S.: On the Equivalence between Radiance and Retrieval Assimilation, *Monthly Weather Review*, 140, 258–265, <https://doi.org/10.1175/MWR-D-10-05047.1>, 2012.
- Miles, G. M., Siddans, R., Kerridge, B. J., Latter, B. G., and Richards, N. A. D.: Tropospheric ozone and ozone profiles retrieved from GOME-2 and their validation, *Atmospheric Measurement Techniques*, 8, 385–398, <https://doi.org/10.5194/amt-8-385-2015>, 2015.

- Miyazaki, K., Eskes, H. J., Sudo, K., Takigawa, M., van Weele, M., and Boersma, K. F.: Simultaneous assimilation of satellite NO₂, O₃, CO, and HNO₃ data for the analysis of tropospheric chemical composition and emissions, *Atmospheric Chemistry and Physics*, 12, 9545–9579, <https://doi.org/10.5194/acp-12-9545-2012>, 2012.
- Munro, R., Lang, R., Klaes, D., Poli, G., Retscher, C., Lindstrot, R., Huckle, R., Lacan, A., Grzegorski, M., Holdak, A., Kokhanovsky, A., Livschitz, J., and Eisinger, M.: The GOME-2 instrument on the Metop series of satellites: instrument design, calibration, and level 1 data processing - an overview, *Atmospheric Measurement Techniques*, 9, 1279–1301, <https://doi.org/10.5194/amt-9-1279-2016>, 2016.
- Parrish, D. F. and Derber, J. C.: The National Meteorological Center's Spectral Statistical-Interpolation Analysis System, *Monthly Weather Review*, 120, 1747–1763, [https://doi.org/10.1175/1520-0493\(1992\)120<1747:TNMCSS>2.0.CO;2](https://doi.org/10.1175/1520-0493(1992)120<1747:TNMCSS>2.0.CO;2), 1992.
- Rodgers, C. D.: Characterization and error analysis of profiles retrieved from remote sounding measurements, *Journal of Geophysical Research (Atmospheres)*, 95, 5587–5595, <https://doi.org/10.1029/JD095iD05p05587>, 1990.
- Rodgers, C. D.: *Inverse methods for atmospheric sounding*, World Scientific Publishing, Singapore, 2000.
- Segers, A. J., Eskes, H. J., van der A, R. J., van Oss, R. F., and van Velthoven, P. F. J.: Assimilation of GOME ozone profiles and a global chemistry-transport model using a Kalman filter with anisotropic covariance, *Quarterly Journal of the Royal Meteorological Society*, 131, 477–502, <https://doi.org/10.1256/qj.04.92>, 2005.
- Sofieva, V. F., Rahpoe, N., Tamminen, J., Kyrölä, E., Kalakoski, N., Weber, M., Rozanov, A., von Savigny, C., Laeng, A., von Clarmann, T., Stiller, G., Lossow, S., Degenstein, D., Bourassa, A., Adams, C., Roth, C., Lloyd, N., Bernath, P., Hargreaves, R. J., Urban, J., Murtagh, D., Hauchecorne, A., Dalaudier, F., van Roozendaal, M., Kalb, N., and Zehner, C.: Harmonized dataset of ozone profiles from satellite limb and occultation measurements, *Earth System Science Data*, 5, 349–363, <https://doi.org/10.5194/essd-5-349-2013>, 2013.
- Uppala, S. M., Kållberg, P. W., Simmons, A. J., Andrae, U., Bechtold, V. D., Fiorino, M., Gibson, J. K., Haseler, J., Hernandez, A., Kelly, G. A., Li, X., Onogi, K., Saarinen, S., Sokka, N., Allan, R. P., Andersson, E., Arpe, K., Balmaseda, M. A., Beljaars, A. C. M., Van De Berg, L., Bidlot, J., Bormann, N., Caires, S., Chevallier, F., Dethof, A., Dragosavac, M., Fisher, M., Fuentes, M., Hagemann, S., Hólm, E., Hoskins, B. J., Isaksen, I., Janssen, P. A. E. M., Jenne, R., McNally, A. P., Mahfouf, J.-F., Morcrette, J.-J., Rayner, N. A., Saunders, R. W., Simon, P., Sterl, A., Trenberth, K. E., Untch, A., Vasiljevic, D., Viterbo, P., and Woollen, J.: The ERA-40 re-analysis, *Quarterly Journal of the Royal Meteorological Society*, 131, 2961–3012, <https://doi.org/10.1256/qj.04.176>, 2005.
- van der A, R. J., Allaart, M. A. F., and Eskes, H. J.: Multi sensor reanalysis of total ozone, *Atmospheric Chemistry and Physics*, 10, 11 277–11 294, <https://doi.org/10.5194/acp-10-11277-2010>, 2010.
- van der A, R. J., Allaart, M. A. F., and Eskes, H. J.: Extended and refined multi sensor reanalysis of total ozone for the period 1970-2012, *Atmospheric Measurement Techniques*, 8, 3021–3035, <https://doi.org/10.5194/amt-8-3021-2015>, 2015.
- van Peet, J. C. A., van der A, R. J., Tuinder, O. N. E., Wolfram, E., Salvador, J., Levelt, P. F., and Kelder, H. M.: Ozone Profile Retrieval Algorithm (OPERA) for nadir-looking satellite instruments in the UV–VIS, *Atmospheric Measurement Techniques*, 7, 859–876, <https://doi.org/10.5194/amt-7-859-2014>, 2014.
- WMO: Implementation plan for the global observing system for climate in support of the UNFCCC (2010 update), Report nr. GCOS-138, Geneva, Switzerland, 2010.
- WOUDC, WMO/GAW: WMO/GAW Ozone Monitoring Community, World Meteorological Organization- Global Atmosphere Watch Program (WMO-GAW)/World Ozone and Ultraviolet Radiation Data Centre (WOUDC) [Data]. Retrieved April 15, 2016, from <http://woudc.org>. A list of all contributors is available on the website., <https://doi.org/10.14287/10000001>, 2016.